Quaternary Science Reviews 126 (2015) 201–218

Contents lists available at ScienceDirect

Quaternary Science Reviews

journal homepage: www.elsevier.com/locate/quascirev

Reconstruction of glacier variability from lake sediments reveals dynamic Holocene climate in Svalbard

Willem G.M. van der Bilt [a, b, *], Jostein Bakke [a, b], Kristian Vasskog [b, c], William J. D'Andrea [d], Raymond S. Bradley [e], Sædis Ólafsdóttir [a, b]

[a] Department of Earth Science, University of Bergen, Allégaten 41, 5007, Bergen, Norway
[b] Bjerknes Centre for Climate Research, Allégaten 55, 5020, Bergen, Norway
[c] Uni Climate, Uni Research, Allégaten 55, 5007 Bergen, Norway
[d] Lamont-Doherty Earth Observatory, Columbia University, Palisades, NY 10964, USA
[e] Department of Geosciences, University of Massachusetts, Amherst, MA 01003, USA

ARTICLE INFO

Article history:
Received 26 May 2015
Received in revised form
24 August 2015
Accepted 1 September 2015
Available online 12 September 2015

Keywords:
Holocene climate
Svalbard
Glacier activity
Lake sediments
Numerical analyses

ABSTRACT

The Arctic is warming faster than anywhere else on Earth. Holocene proxy time-series are increasingly used to put this amplified response in perspective by understanding Arctic climate processes beyond the instrumental period. However, available datasets are scarce, unevenly distributed and often of coarse resolution. Glaciers are sensitive recorders of climate shifts and variations in rock-flour production transfer this signal to the lacustrine sediment archives of downstream lakes. Here, we present the first full Holocene record of continuous glacier variability on Svalbard from glacier-fed Lake Hajeren. This reconstruction is based on an undisturbed lake sediment core that covers the entire Holocene and resolves variability on centennial scales owing to 26 dating points. A toolbox of physical, geochemical (XRF) and magnetic proxies in combination with multivariate statistics has allowed us to fingerprint glacier activity in addition to other processes affecting the sediment record. Evidence from variations in sediment density, validated by changes in Ti concentrations, reveal glaciers remained present in the catchment following deglaciation prior to 11,300 cal BP, culminating in a Holocene maximum between 9.6 and 9.5 ka cal BP. Correspondence with freshwater pulses from Hudson Strait suggests that Early Holocene glacier advances were driven by the melting Laurentide Ice Sheet (LIS). We find that glaciers disappeared from the catchment between 7.4 and 6.7 ka cal BP, following a late Hypsithermal. Glacier reformation around 4250 cal BP marks the onset of the Neoglacial, supporting previous findings. Between 3380 and 3230 cal BP, we find evidence for a previously unreported centennial-scale glacier advance. Both events are concurrent with well-documented episodes of North Atlantic cooling. We argue that this brief forcing created suitable conditions for glaciers to reform in the catchment against a background of gradual orbital cooling. These findings highlight the climate-sensitivity of the small glaciers studied, which rapidly responded to climate shifts. The start of prolonged Neoglacial glacier activity commenced during the Little Ice Age (LIA) around 700 cal BP, in agreement with reported advances from other glaciers on Svalbard. In conclusion, this study proposes a three-stage Holocene climate history of Svalbard, successively driven by LIS meltwater pulses, episodic Atlantic cooling and declining summer insolation.

1. Introduction

Instrumental observations suggest that the Arctic has been changing faster than any other region on the Northern hemisphere over the past decades (Serreze and Barry, 2011). This amplified response has consistently been simulated by climate models for a future with increased atmospheric greenhouse gas concentrations (Pithan and Mauritsen, 2014). But though albedo and temperature feedbacks have been suggested (Screen and Simmonds, 2010), the drivers of Arctic climate variability have yet to be fully constrained (Miller et al., 2010). It is important to improve our understanding of

* Corresponding author. Department of Earth Science, University of Bergen, Allégaten 41, 5007, Bergen, Norway.
E-mail address: willemvanderbilt@gmail.com (W.G.M. van der Bilt).

http://dx.doi.org/10.1016/j.quascirev.2015.09.003

forcing mechanisms, as the Arctic has a disproportionately large influence on global climate (McGuire et al., 2006; Solomon, 2007). As the paradigm of a stable Holocene climate has shifted (Bond et al., 2001; Overpeck et al., 1997), Holocene proxy time-series are increasingly considered as potential analogues for future climate, and may help assess the range of natural Arctic climate variability (McKay and Kaufman, 2014; Wanner et al., 2011).

However, Arctic climate proxy datasets are scarce and unevenly distributed (Wanner et al., 2011). Moreover, records often cover only parts of the Holocene and lack robust chronological control (Sundqvist et al., 2014). Continuous, well-dated and high-resolution archives are required to resolve the temporal and spatial signature of Holocene Arctic climate variability. Glaciers are ubiquitous in the Arctic and rapidly respond to shifts in summer temperature and winter precipitation (Oerlemans, 2005; Østrem and Liestøl, 1964). This sensitive response to climate change is captured by variations in minerogenic rock-flour production and may be recorded in lacustrine sediment archives of downstream glacier-fed lakes (Karlén, 1976, 1981). Monitoring data demonstrate that variations in the flux of minerogenic sediments into glacier-fed lakes provide a robust high-resolution record of glacier activity and size (Leemann and Niessen, 1994a; Liermann et al., 2012; Roland and Haakensen, 1985). The signature of rock-flour in lacustrine sediments therefore serves as a climate proxy that has been widely applied (Bakke et al., 2010; McKay and Kaufman, 2009; Rosqvist and Schuber, 2003; Simonneau et al., 2014). Indeed, sediment records from glacier-fed lakes are rated among the best continuous high-resolution terrestrial proxy archives available (Ashley, 1995; Carrivick and Tweed, 2013). Here, the conceptual model described above has been further developed into a multi-proxy approach that integrates physical (Bakke et al., 2005), magnetic (Paasche et al., 2007) and geochemical tools (Bakke et al., 2009), in combination with numerical techniques (Bakke et al., 2013; Vasskog et al., 2012).

We present a sediment record from glacier-fed Lake Hajeren in northwest Spitsbergen that encompasses the entire Holocene. This region sits at the crossroads of Arctic and Atlantic water masses and is therefore sensitive to climate shifts (Rasmussen et al., 2014; Werner et al., 2013). Nonetheless, the coverage of high-resolution terrestrial climate proxy records in the area is sparse. The main goal of this study is to provide a reconstruction of Holocene glacier activity that will improve our understanding of centennial-scale Arctic climate variability. To this end, we apply a multi-proxy toolbox to ensure rigor in our interpretations. The methods also enable us to detect other catchment and lake processes that leave an imprint in the lake sediment record. Accurate detection of sediments reflecting glacier activity requires a full understanding of these processes, which include, but are not limited to, paraglacial redeposition (Ballantyne, 2002), mass wasting (Vasskog et al., 2011), lake stratification (Leemann and Niessen, 1994a; Richards et al., 2012) and redox processes (Lamoureux and Gilbert, 2004). Moreover, to ensure the chronological robustness required to resolve centennial climate variability (Sundqvist et al., 2014), we have used a combination of radiocarbon dating and Paleomagnetic Secular Variations (PSV). Finally, we integrate this study into a regional paleoclimatic context by comparing our site-specific findings to other high-resolution proxy records from the Arctic sector of the North-Atlantic.

2. Setting

Hajeren, the distal glacier-fed lake investigated in this study, measures 0.23 km^2 and is located on the Mitrahalvøya Peninsula in Northwest Spitsbergen (79°15′33.47″N 11°31′4.25″E) (Fig. 1). Bathymetric profiling reveals two basins with a maximum depth of 19.5 m (Fig. 2). The lake's surface elevation is 35 m a.s.l., placing Hajeren slightly above the local marine limit reported by Landvik et al. (2013) (32 m a.s.l.).

The catchment of Lake Hajeren covers 2.96 km^2 of which 0.25 km^2 is presently glacier-covered. Two northwest-facing cirque glaciers drain into the lake (Fig. 1), which will henceforth be referred to as North and South glaciers. Based on field observations (Van der Bilt et al., 2015), the North Glacier (0.8 km^2) is believed to be polythermal, while the South Glacier (0.17 km^2) may have turned cold-based due to recent thinning. Based on documented past glacier front positions (NPI, 2015) and a lack of geomorphic evidence (e.g. tectonised sediments and looped moraines), we argue that both glaciers are not surging. Also, using a historical aerial photographs (NPI, 1936), both have been retreating for at least 78 years and likely since the Little Ice Age (LIA). This period of favorable conditions for glacier growth commenced after 1.3 ka cal BP and culminated on Svalbard during the 19th century (Salvigsen and Høgvard, 2006). Lake Hajeren is drained by an ephemeral spillway, enhancing its capacity to retain glacigenic suspended load (Dahl et al., 2003).

The glacial geomorphology of the catchment is characterized by two sets of terminal moraine deposits that are indicated as stages 1 and 2 in Fig. 1. Based on aerial photographs from 1936 (NPI, 1936), Stage 2 moraines were deposited during the culmination of the Little Ice Age (LIA). The more distal Stage 1 moraines are exclusively found in front of the more erosive polythermal North glacier and comprise a complex of mounds (Van der Bilt et al., 2015). Their weathered appearance and position outside Stage 2 moraine deposits suggests that they were possibly deposited during a pre-LIA glacier maximum, in agreement with findings from nearby catchments (Reusche et al., 2014; Røthe et al., 2015).

Bedrock geology comprises Proterozoic protoliths of the Krossfjorden group that were metamorphosed during the Grenvillian orogeny (Dallmann, 2015). Local bedrock predominantly consists of NNW–SSE trending Signehamna formation schists that are horizontally overlain by marble belonging to the Generalfjellet formation in southern Mitrahalvøya (Krasilščikov, 1975).

Climate in Spitsbergen is influenced by the West and East Spitsbergen currents (Rasmussen et al., 2014). The former transports warm and saline Atlantic waters northwards (Aagaard-Sørensen et al., 2014), while the latter brings in cold water from the Arctic Ocean (Loeng, 1991). The interplay between these distinctly different water masses create a climate that is highly sensitive to shifting oceanic and atmospheric conditions (Rasmussen et al., 2014) as well as changes in sea ice extent (Benestad et al., 2002; Müller et al., 2012). At present, Northwest Spitsbergen has a maritime polar climate with an average annual temperature of −5 °C and 427 mm of annual precipitation measured at nearby Ny Ålesund for the 1980–2010 period (Førland et al., 2012). Temperatures have been recorded since 1898 and reveal highly variable, but generally warming conditions during the 20th century (Nordli et al., 2014). Moreover, the last 30 years are characterized by continuous warming with the warmest years on record occurring during the past decade (Nordli, 2010).

3. Material & methods

3.1. Coring and mapping

In August 2012, a seismic survey was carried out on Lake Hajeren, using a Malå Ground Penetrating Radar (GPR) system fitted with a 50 Mhz antenna. Post-processing of these data using the RadExplorer software package revealed a fairly homogeneous distribution of soft sediments over two sub-basins henceforth referred to as North and South basins, with water depths of 13 and

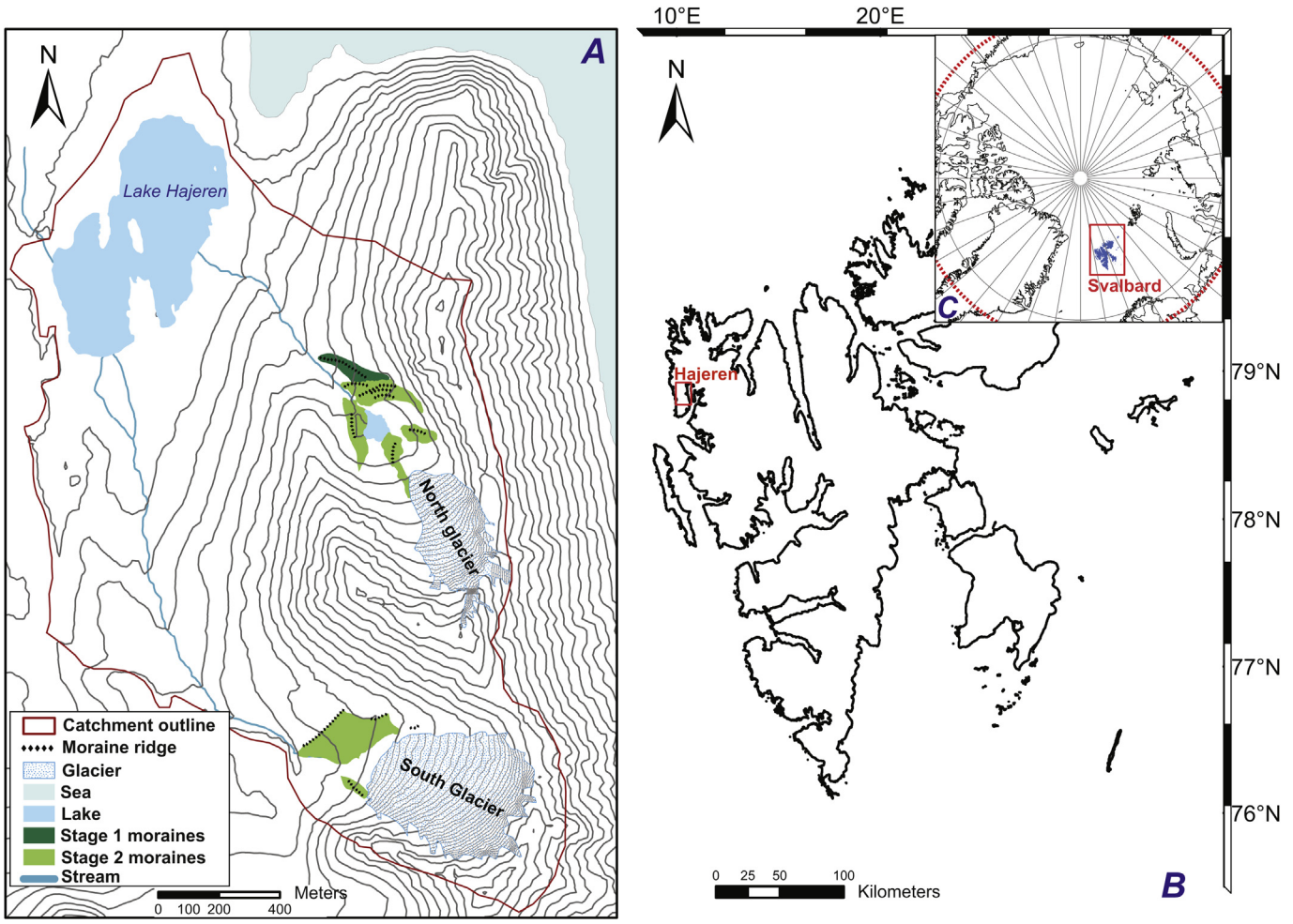

Fig. 1. A: A simplified 25 m contour geomorphological map of the Hajeren catchment, outlined by a red line. Both North and South glaciers, their outlet streams and lake Hajeren are displayed. B: Close-up of the Svalbard archipelago, marking the Hajeren catchment with a red rectangle. C: North Pole view map of Svalbard (blue) and the Arctic (delimited by the red dashed line). (For interpretation of the references to color in this figure legend, the reader is referred to the web version of this article.)

19.5 m, respectively (Figs. 2 and 3). Following the seismic survey, sediment cores were extracted close to the deepest spots in each basin (Fig. 3). Fig. 2 demonstrates that the lake bottom surrounding both coring sites is flat, reducing the risk of post-depositional sediment disturbance like slumping (Dahl et al., 2003). Two cores, HAP0112 and HAP0212, were extracted from a coring platform, using a modified Nesje piston corer (Nesje, 1992) fitted with 110 mm diameter tubing (Fig. 3). Coring was followed by geomorphological mapping during the summer of 2014. Landform-sediment assemblages in the catchment have subsequently been mapped at in detail (Van der Bilt et al., 2015), complimenting evidence from aerial photographs (NPI, 1936, 2009).

3.2. Analyses

We reconstructed glacier activity in the Hajeren catchment using a combination of geomorphological mapping, lake coring, and laboratory analyses of the lake sediments. The latter encompass a toolbox of physical, geochemical and magnetic proxies, developed to detect a glacier signal in distal glacier-fed lakes (Bakke et al., 2013; Røthe et al., 2015; Wittmeier et al., 2015). A robust chronology was established using Accelerator Mass Spectrometry (AMS) radiocarbon dating of terrestrial macrofossils and Paleomagnetic Secular Variations (PSV).

3.2.1. Lithostratigraphy

Before describing their lithological characteristics, the extracted piston cores were split. Sediments from core HAP0112, extracted adjacent to a steep slope in the South basin, were found to be disturbed between 35 and 125 cm core depth (Fig. 3). As such, the 332 cm long undisturbed core HAP0212 from the North basin of Lake Hajeren was selected as master core (Figs. 3 and 4). Moderate correspondence with the undisturbed upper 35 cm of HAP0112, using Zr counts, suggests that the sedimentary signal from HAP0212 is representative (Fig. 3). To measure sediment Dry Bulk Density (DBD), indicative for the influx of suspended rock-flour (Karlén, 1976) and a proxy for glacier activity (Bakke et al., 2005),0.5 cm^3 of sediment was extracted every 0.5 cm ($n = 618$). The bottom 20 cm of HAP0212 comprises a pebbly diamict and could therefore not be sampled. Samples were subsequently dried overnight at 105 °C and weighted for DBD and Water Content (WC) following Menounos (1997). To measure organic content, the same samples were subsequently transferred to crucibles and ignited at 550 °C for Loss-On-Ignition (LOI) in a muffle furnace (Heiri et al., 2001).

3.2.2. Magnetic properties

Mineral magnetic properties are commonly used as indicators of glacially-derived minerogenic matter in the sedimentary record of

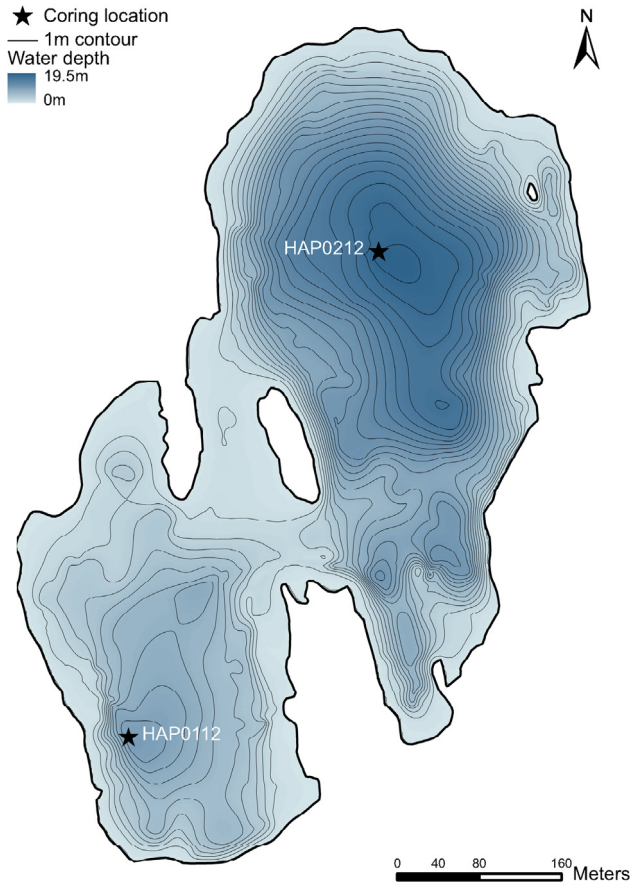

Fig. 2. Bathymetry of Lake Hajeren with 1 m contour lines, showing two sub-basins. Coring locations of cores HAP0112 and HAP0212 are indicated.

glacier-fed lakes (Matthews and Karlén, 1992; Snowball and Sandgren, 1996). For this study, we measured surface Magnetic Susceptibility (MS) and (bulk) Anhysteric Remanent Magnetization ((χ)ARM) on HAP0212. Surface MS was measured continuously at 1 cm resolution with a Bartington MS3 meter equipped with a MS2E surface sensor. ARM was first measured on extracted u-channels at 1 cm intervals in a 2G superconducting rock magnetometer at Oregon State University by applying a 0.1 mT Direct Current (DC) field followed by a 10 mT Alternating Current (AC) field. To allow for a more detailed investigation of the variable upper core half, we also measured bulk ARM (χARM) on 6 cm^3 discrete samples extracted at 0.5 cm intervals (n = 327). To this end, we imposed identical DC and AC field strengths in a 2G Alternating Field (AF) degausser.

3.2.3. Geochemistry

X-Ray Fluorescence (XRF) count rates detect changes in lithogenic influx and have been used to infer changes in glacier mass turnover (Bakke et al., 2009). Accordingly, the geochemistry of HAP0212 was semi-quantitatively mapped using an XRF core scanner (Croudace et al., 2006). Elemental profiles were obtained at 200 μm resolution from the split cores by a Cox Analytical Systems ITRAX scanner at the department of Earth Science in Bergen. To acquire the highest sensitivity for heavier lithogenic elements, scans were performed using a Molybdenum (Mo) tube (Boës et al., 2011). The cores were covered with foil to prevent sediments from drying out and protect the detector of the instrument after Tjallingii et al. (2007). To prevent interannual variability from obscuring the centennial-scale climate signal studied here (Birks, 1998), measurements were smoothed using a 25-point moving average and subsequently resampled at 0.5 cm resolution.

3.2.4. Chronology

We used two independent chronological methods to construct an age-depth model for core HAP0212: radiocarbon dating and Paleomagnetic Secular Variation (PSV) correlation. 24 terrestrial plant macrofossil samples were extracted at frequent intervals by wet-sieving sediments using a 125 μm mesh, transferred to sterile vials and submitted for AMS radiocarbon dating (Table 1). Samples with a dry weight equal or less than 2 mg (n = 13) were sent to the Lund University Radiocarbon Dating Laboratory (LuS). Larger samples (n = 11) were processed by the Poznan Radiocarbon Laboratory (Poz). PSV describe the directional and intensity changes of Earth's magnetic field and enables chronological synchronization between records (Thompson and Turner, 1979). To improve chronological accuracy, we used a PSV-derived chronology for core sections below 231.5 cm depth, characterized by the infrequent and scarce occurrence of datable macrofossils (Table 1). We could not extract material for basal dating from both units 4 and 5 in the absence of macrofossils. Declination, inclination and intensity component records were measured on core HAP0212 at 1 cm resolution, using a 2G superconducting rock magnetometer at Oregon State University (Ólafsdóttir et al., in prep.). Tie-points were then generated by synchronizing HAP0212 inclination and declination features to those of the well-dated MD99-2269 marine core from the Icelandic shelf (Ólafsdóttir et al., 2013; Stoner et al., 2007).

3.2.5. Grain size

As glacial meltwater is characterized by an abundance of suspended silt and clay grains (1–63 μm) (Leemann and Niessen, 1994a), we analyzed the grain-size distribution of selected minerogenic intervals. 8–12 gr of sediment were extracted every 1 cm for the intervals between 39.5 and 47.5 (1), 110.5–115.5 (2) and 137.5–144.5 (3) cm core depth (n = 36). The same was done between 30.5 and 34.5 cm (n = 5), the onset of a period of sustained minerogenic sedimentation and documented LIA glacier activity (paragraph 2) To dissolve organic matter, sediment samples were stirred for 2 days in a 5% H_2O_2 aqueous solution before being sieved through a 63 μm mesh. The dried residue was then disaggregated in a 0.005% Calgon solution (Jones et al., 1988) and analyzed in a Micromeritics Sedigraph 5100 equipped with a Mastertech 5.1 automatic sampler. We employed the GRADISTAT grain size statistics package by Blott and Pye (2001) to process Sedigraph measurements using the geometric Folk and Ward method (Folk and Ward, 1957).

3.2.6. Statistics

Statistical analyses are increasingly applied on lake sediment records to improve our understanding of multi-proxy datasets (Birks, 1998; Koinig et al., 2003). Here, we applied cluster analysis on the HAP0212 dataset to objectively categorize the record into different units, while normalization against LOI was used to account for dilution effects in the geochemical data. Finally, ordination was performed using Principal Component Analysis (PCA) in order to investigate variability shared between proxies.

3.2.6.1. Cluster analysis. Lake sediment records are commonly categorized into stratigraphical units using subjective methods such as visual inspection. Here, cluster analysis was applied to objectively categorize the HAP0212 record into different units. Following Bakke et al. (2013), we used the constrained incremental sum of squares clustering (CONISS) algorithm (Grimm, 1987) in the Tilia software package (Grimm, 2011). The independently measured parameters ARM, DBD and MS were selected for cluster

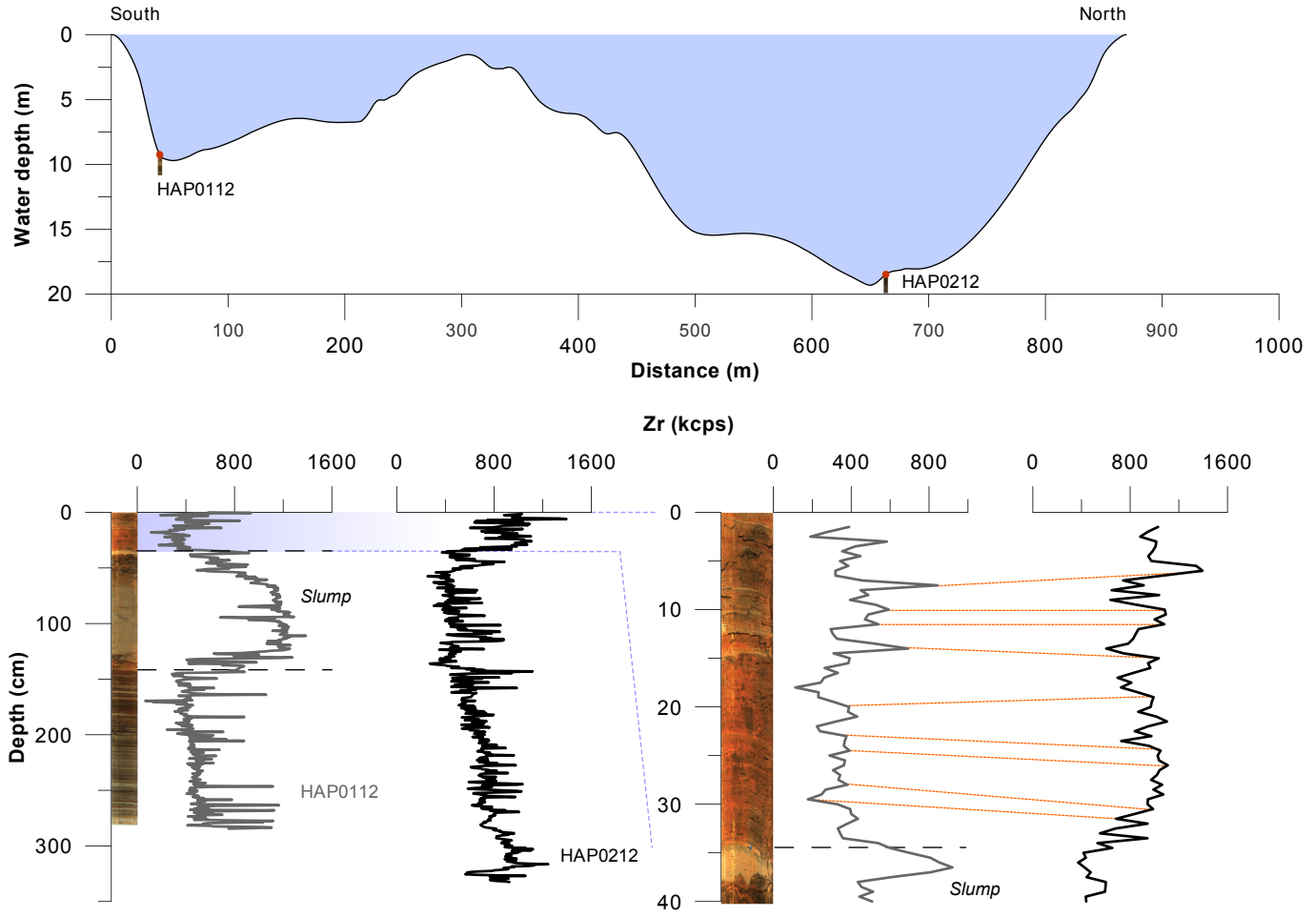

Fig. 3. Transect through both South and North basins of Lake Hajeren. Coring locations of HAP0112 and HAP0212 are indicated. The upper 40 cm of both cores have been correlated using Zr count rates.

analysis. Dissimilarity was then calculated using Euclidean distance and expressed using total mean square values. We took a total sum of squares cut-off value of 1.25 to subdivide the record.

3.2.6.2. Normalization. Elemental profiles measured by XRF core scanner are affected by physical sediment properties (Croudace et al., 2006) and should therefore be cautiously interpreted. For this study, we used normalization to address impacts of the commonly described closed-sum effect (Rollison, 1993), which concerns dilution of the XRF signal by organic matter. This may obscure relative changes in elemental abundances and could therefore overprint sources of environmental variability in our data that are unrelated to changing organic content.

We first applied multiple criteria for the selection of XRF elemental profiles in our analysis. Only elements with high sensitivity to the Mo tubing fitted during measurement were included according to Cox Analytical Systems specifications. This selection excludes lighter elements that are known to be sensitive to scattering and absorption of X-rays by water, such as Al and Si (Tjallingii et al., 2007). Moreover, elements with low count rates, here defined as having a mean < 100 kilocounts per second (kcps), were omitted following Striberger et al. (2011). Finally, we excluded elements with a low signal-to-noise ratio (SNR), defined as the ratio of mean μ over standard deviation σ after Montgomery (2008), equal or less than 2.

Different approaches that aim to resolve the closed-sum effect on scanning XRF data through normalization have been proposed. For example, Thomson et al. (2006) and Löwemark et al. (2011) suggest normalizing against conservative Al. Kylander et al. (2011), on the other hand, normalize their data against the ratio of incoming plus coherent scattering, which responds to shifts in organic content. Here we adopted a variation of the latter approach, normalizing conservative elements against our separately measured LOI record. Normalizing against LOI enables us to isolate environmental variability not related to changes in organic content of the sediments. This step is expected to amplify the subtle shifts in minerogenic input characteristic for changes in the mass turnover rate of small glaciers like those in the study area (Leonard, 1985).

3.2.6.3. Ordination. Ordination techniques have been increasingly employed to understand gradients of environmental variation in lake sediment core data since the 1980s (Sergeeva, 1983). Following Vasskog et al. (2012), we carried out Principal Component Analysis (PCA) (Hotelling, 1933) on our multi-proxy dataset to assess whether variables show a shared response to glacigenic sedimentation. To this end, we used version 5 of the CANOCO software by Ter Braak (1988). Assessed variables were transformed prior to PCA to reduce the asymmetry of their distribution and increase linearity (Legendre and Birks, 2012), following CANOCO suggestions. Non-linearity between variables reduces the common variability detected by PCA and renders the ordination axes dependent

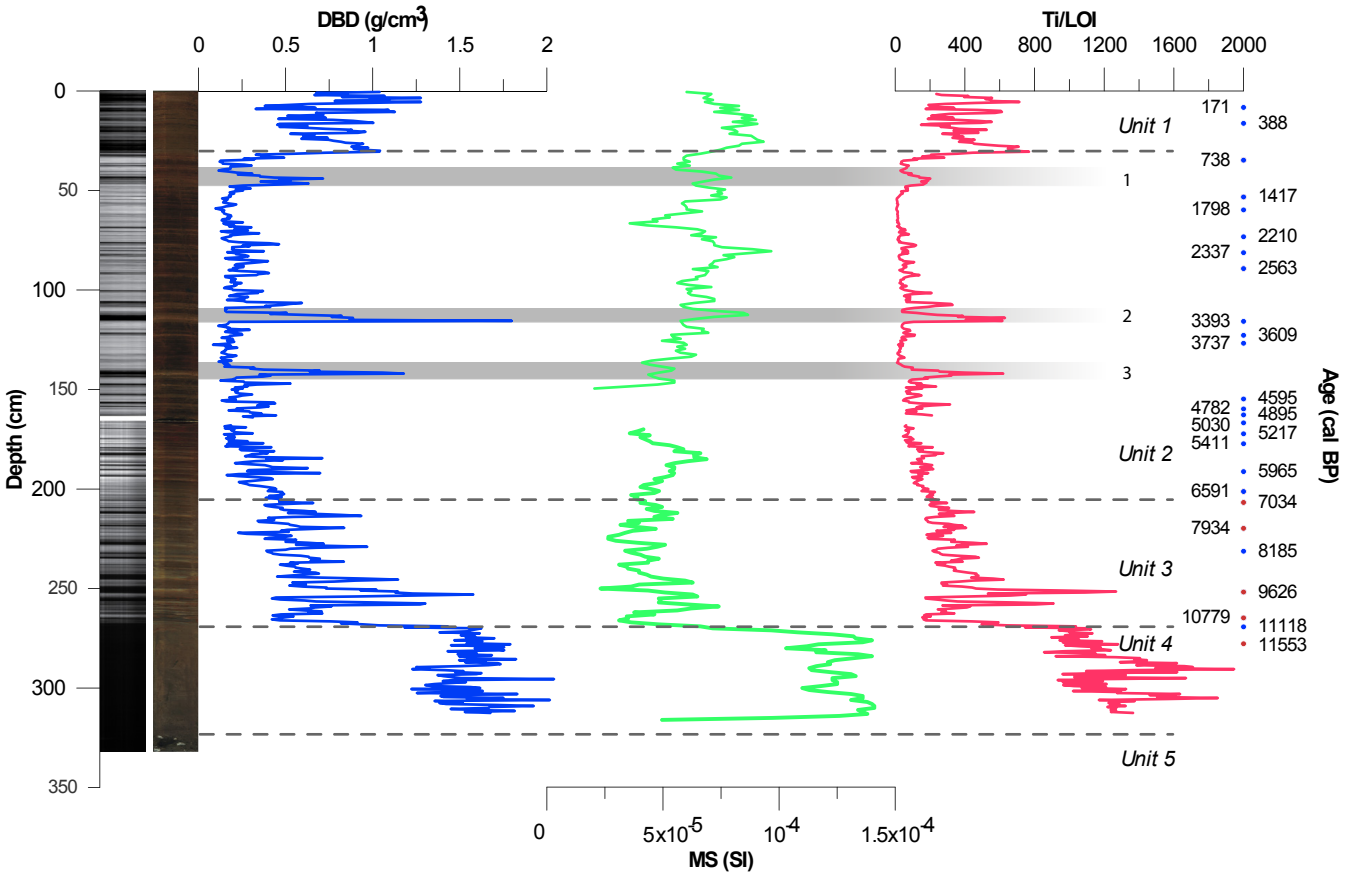

Fig. 4. Minerogenic (glacigenic) indicators DBD and Ti/LOI as well as MS from core HAP0212, plotted on depth-scale at 0.5 cm resolution. The 4 main units, determined by cluster analysis (paragraph 3.2.6.1) are delimited with dashed lines. Intervals 1, 2 and 3 are emphasized by shaded bars. Optical (RGB) and radiograph grayscale images are displayed on the left, while the core depths (red bullets) and calibrated ages of dated samples are shown on the right. (For interpretation of the references to color in this figure legend, the reader is referred to the web version of this article.)

(Šmilauer and Lepš, 2014). To emphasize correlations in the ordination diagram, variables were respectively centered and standardized before analysis, following the recommendations of Šmilauer and Lepš (2014). Based on the previously described criteria, 9 variables were included in the PCA on a shared 1-cm sampling resolution (n = 250): elemental count rates of K, Ti, Fe,

Table 1
Overview of radiocarbon samples from core HAP0212.

Core	Lab nr.	Material	mg C	Depth (cm)	^{14}C age (BP)	Min. age (cal BP)	Max. age (cal BP)	Mean (cal BP)
HAP0212 1-2	Poz-57711	Plant macrofossil	0.5	8.5	175 ± 25	137	223	171
HAP0212 1-2	Poz-57712	Plant macrofossil	0.4	16.5	350 ± 40	313	493	388
HAP0212 1-2	LuS 10735	Plant macrofossil	0.19	35	800 ± 60	658	802	738
HAP0212 1-2	LuS 10736	Plant macrofossil	0.3	53.5	1470 ± 50	1293	1418	1417
HAP0212 1-2	LuS 10737	Plant macrofossil	0.22	60	1935 ± 60	1722	2000	1798
HAP0212 1-2	Poz-57713	Plant macrofossil	0.3	73.5	2200 ± 50	2109	2339	2210
HAP0212 1-2	Poz-57714	Plant macrofossil	0.5	81.5	2305 ± 35	2301	2360	2337
HAP0212 1-2	LuS 10738	Plant macrofossil	0.42	89.5	2500 ± 50	2426	2743	2563
HAP0212 1-2	LuS 10739	Plant macrofossil	0.44	116	3175 ± 50	3322	3484	3393
HAP0212 1-2	LuS 10740	Plant macrofossil	0.36	123	3355 ± 50	3461	3699	3609
HAP0212 1-2	LuS 10741	Plant macrofossil	0.36	127	3480 ± 50	3633	3879	3737
HAP0212 1-2	Poz-57715	Plant macrofossil	0.4	155	4070 ± 40	4436	4649	4595
HAP0212 1-2	LuS 10742	Plant macrofossil	0.48	160	4230 ± 50	4611	4767	4782
HAP0212 1-2	Poz-57716	Plant macrofossil	0.8	163	4370 ± 35	4856	4984	4895
HAP0212 2-2	Poz-60452	Plant macrofossil	0.6	167	4425 ± 35	4872	5069	5030
HAP0212 2-2	Poz-60453	Plant macrofossil	0.7	172.5	4480 ± 35	5035	5291	5217
HAP0212 2-2	Poz-60454	Plant macrofossil	0.6	177.5	4720 ± 40	5324	5416	5411
HAP0212 2-2	Poz-60455	Plant macrofossil		191.5	5200 ± 35	5903	6004	5965
HAP0212 2-2	Poz-60456	Plant macrofossil	0.4	201.5	5770 ± 50	6446	6672	6591
HAP0212 2-2	LuS 10866	Plant macrofossil	0.4	231.5	7305 ± 50	8004	8200	8185
HAP0212 2-2	LuS 10867	Plant macrofossil	0.3	248.5	9565 ± 55	10,715[a]	11,109[a]	10,912[a]
HAP0212 2-2	LuS 10868	Plant macrofossil	0.2	265.5	16,580 ± 180	*	*	*
HAP0212 2-2	LuS 10869	Plant macrofossil	0.4	269.5	9750 ± 55	11,082	11,254	11,118
HAP0212 2-2	LuS 10870	Plant macrofossil	0.3	317	25,100 ± 300	*	*	*

*Indicate samples that were not calibrated due to an improbable age (LuS 10868) and extracted from the disturbed lower core section (LuS 10870).
[a] Indicate designated outliers.

Rb and Zr in addition to the physical parameters DBD and LOI as well as magnetic properties ARM and MS.

4. Results

4.1. Lithostratigraphy

The lithostratigraphy of core HAP0212 is shown in Figs. 4 and 5. By means of cluster analysis, the upper 320 cm of the record were objectively categorized into four units (1–4). The bottom 20 cm of HAP0212 (unit 5) was too coarse-grained and uneven for sampling or scanning and is therefore also excluded from cluster analysis.

4.1.1. Unit 5 (332 – 320 cm)

Unit 5 encompasses the bottom 12 cm of core HAP0212 and comprises two sub-units, 5a and 5b. 5a (332–323.5 cm) is a diamict that consists of sub-angular pebble-sized clasts with no apparent orientation, embedded in a matrix of grey silty clay with a 2.5Y 6/2 Munsell chart value (Munsell and Color, 2000). The embedded clasts all consist of mica schist, similar to the Signehamna formation bedrock found in the Hajeren watershed (Ohta et al., 2002). The angular open work fine gravels of sub-unit 5b (320–323.5 cm) are poorly sorted and fine upwards. The transition into unit 4 is abrupt along a truncated surface.

4.1.2. Unit 4 (320 – 272 cm)

Unit 4 consists of massive grey (2.5Y 7/2) sandy silts with high DBD values that average 1.55 g/cm^3 (Fig. 4). We measured undrained shear strength of 126 kPa in duplicate at 300 cm core depth using a fall cone test after Tanaka et al. (2012), suggesting compaction. Dewatering structures are also visible at selected intervals. In its entirety, unit 4 is faintly stratified, as the silty fining-upwards sediments are regularly interspersed with sandier intervals.

4.1.3. Unit 3 (272 – 203 cm)

Fig. 4 shows that the physical characteristics of units 3 and 4 differ significantly. The faint laminations in the upper part of unit 4 become more apparent in unit 3 due to more distinct variations in minerogenic content reflected by LOI and DBD curves (Figs. 4 and 5). The lower 10 cm of unit 3 consist of dark brown (7.5YR 4/3) organic-rich sediments and show a marked prolonged spike in LOI with maximum values of 10.5% (Fig. 5). In general, unit 3 is characterized by gradual but distinct alternations between grey (10YR 8/1) minerogenic (LOI ≈ 1.5–5%) and relatively organic-rich dark brown (7.5YR 6/3) intervals (LOI ≈ 5–11%). DBD values peak around 251 cm depth (Fig. 4). Towards the upper boundary, unit 3 grades into dark brown gyttja with a consistently higher organic content.

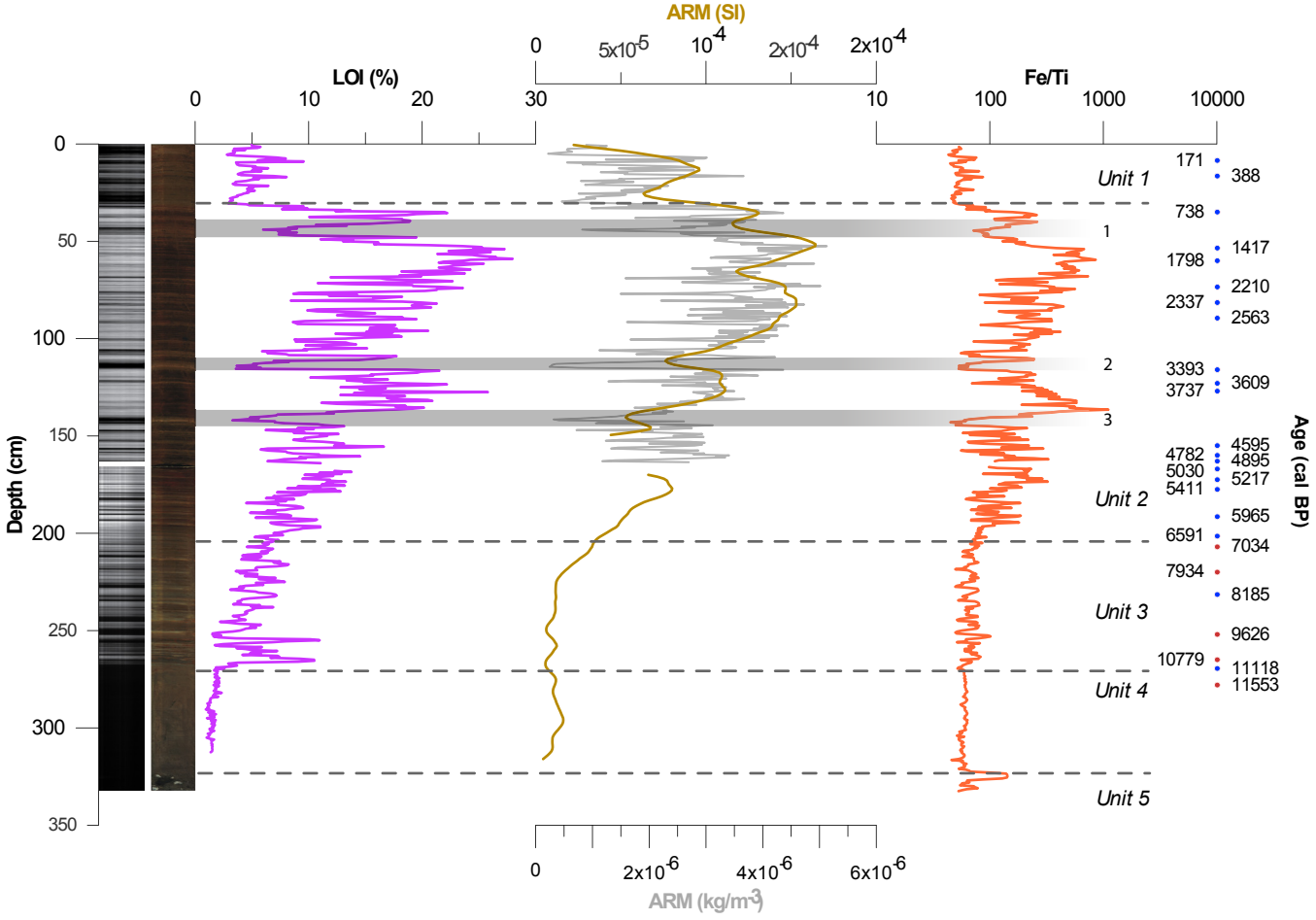

Fig. 5. LOI and ARM, scanned ARM (brown), χARM (grey), and Fe/Ti (orange) from core HAP0212, plotted on depth-scale at 0.5 cm resolution on depth-scale. The 4 main units, determined by cluster analysis (paragraph 3.2.6.1) are delimited with dashed lines. Intervals I, 2 and 3 are emphasized by shaded bars. Optical (RGB) and radiograph grayscale images are displayed on the left, while core depths (red bullets) and calibrated ages of dated radiocarbon samples (blue) as well as PSV tie-points (red) are shown on the right. (For interpretation of the references to color in this figure legend, the reader is referred to the web version of this article.)

4.1.4. Unit 2 (203–30.5 cm)

Unit 2 is characterized by a prolonged increase in LOI values as shown in Fig. 5. This rise in organic content is asymmetrically shaped with a slow build-up from ≈5% towards ≈28% peak at 69 cm depth followed by a rapid decline towards unit 1. Low DBD values suggest minimal minerogenic and/or high organic sedimentation throughout most of unit 2. This trend is interrupted by intervals 1, 2 and 3, as shown in Fig. 5.

The organic-rich sections (LOI > 10%) are colored dark brown (7.5YR 2.5/1), whereas intervals 1, 2 and 3 are yellowish grey (10YR 7/3). The sediments of unit 2 are laminated throughout, but layer properties differ substantially between organic-rich and minerogenic intervals. The former comprise millimeter-scale couplets, while laminae in the latter are substantially wider. Fig. 4 demonstrates that DBD values change rapidly towards the boundary with unit 1, marking a shift towards increasingly minerogenic lacustrine sedimentation.

4.1.5. Unit 1 (30.5–0 cm)

The upper unit of core HAP0212 covers the first period of prolonged minerogenic sedimentation since unit 3. Sediments comprises grey (10 YR 7/1–2) silty clays, comparable to those found in unit 3. Moreover, the grayscale image shows that unit 1 also exhibits the centimeter-scale laminations found in unit 3 and intervals 1, 2 and 3 in unit 2. After spiking at the onset of unit 1, DBD values gradually increase towards the top and peak around 4 cm depth at 1.27 g/cm3. This value is similar to those observed in unit 3 as well as intervals 1, 2 and 3 as shown by Fig. 4.

4.2. Age-depth model

The HAP0212 age-depth model was generated using the Clam 2.2 package (Blaauw, 2010), ran in the open-source R environment version 3.0.1 (RCoreTeam, 2014). Included radiocarbon ages (n = 21) were calibrated using the IntCal13 terrestrial calibration curve for the Northern Hemisphere (Reimer et al., 2013). Based on outlined signs of reworking and a dynamic sedimentology (paragraph 4.12.), sections unit 4 that are older than 11,480 cal BP were excluded from our age-depth model. This basal age was generated through synchronization of the Hajeren PSV record with that of the well-dated master curve from core MD99-2269 (Ólafsdóttir et al., 2013; Stoner et al., 2007). Due to the outlined scarcity of macrofossils and conflicting ages (Table 1), PSV ties were used to constrain our model below 231.5 cm core depth. In total, we admitted 5 points with ages of 7019, 8115, 9639, 10,718 and 11,480 cal BP (Fig. 6). To account for uncertainties, we applied a ±100 years uncertainty envelope after Larsen et al. (2012). Based on the PSV chronology, radiocarbon dates LuS 10867 and LuS868 (Table 1) were designated as an outlier. The final age-depth model was generated using default smooth spline interpolation, producing the highest goodness-of-fit (11.44) (Fig. 6). Ages were interpolated at the common 0.5 cm resolution of our proxy data using 10,000 iterations, as recommended by Blaauw (2010). The resulting age-depth model has an average down-core sample resolution *R* of 21.91 years, with an average dating sample frequency *f* of 421.56 years (Sundqvist et al., 2014).

4.3. Grain size

Clay and silt (1–63 μm) fractions from the previously described minerogenic intervals 1, 2 and 3 were analyzed to help identify their depositional signature (Fig. 7). Additionally, grain size analysis was performed on reference sediments, deposited during the onset of a period of documented glacier activity (paragraph 2). As can be seen in Fig. 7, minerogenic intervals 1, 2 and 3 are dominated by the fine silt and clay fractions. A similar development can be observed for the onset of prolonged late Holocene minerogenic sedimentation in Hajeren at the top of unit 2. Coarser fractions, which often characterize mass-wasting events (Rubensdotter and Rosqvist, 2009; Vasskog et al., 2011), are under-represented in intervals 1, 2 and 3. The grain size distribution profiles also indicate weak bimodality for the discussed intervals with peaks in the (very) fine silt fractions. Finally, Fig. 7 shows that distribution patterns from the latter intervals correspond to those seen for the minerogenic reference sediments of LIA age that border unit 1.

4.4. Magnetic properties

MS and ARM were measured on HAP0212 to track glacier-derived minerogenic sedimentation in Hajeren following Snowball and Sandgren (1996) and Matthews and Karlén (1992). Figs. 4 and 5 show down-core variations in (X)ARM and MS. MS values are highest in the coarse sediments of unit 4 (Fig. 4). Average MS values of unit 4 are 56% higher than those of unit 1, which has the second-highest MS values of HAP0212. Based on the MS measurements, unit 4 appears distinctly different from the other units. It is also apparent that MS and DBD visually correlate in the minerogenic units 1 and 4. This relationship is less visible in unit 3 and poor in unit 2 as demonstrated by a Spearman's rho (ϱ) of 0.316 (n = 130). MS values show a similar asymmetric increase towards the top of unit 2 as observed in the LOI record. Fig. 5 demonstrates this pattern is more pronounced in the ARM record of unit 2. A ϱ of 0.67 (n = 256) between LOI and discrete ARM measurements on unit 2 (XARM) affirms the strength of this correlation. However, as with the previously described LOI record, the build-up of ARM through unit 2 is disrupted by intervals 1, 2 and 3. Following Paasche et al. (2004), XARM was plotted against LOI to investigate the relationship between the two variables through unit 2 in closer detail (Fig. 8). Units 1 and 2 form distinct populations, characterized by different relationships between LOI and ARM as underlined by disparate regression coefficients. Though R^2 values attest to a fairly scattered sample distribution, the trends show that LOI and XARM exhibit a positive relationship with an inflection around 5–10% LOI. XARM and LOI increase congruously throughout unit 2 and high values of both parameters co-occur. However, this relation is markedly different for the low LOI values of minerogenic unit 1. Here, XARM values are an order of magnitude lower. Fig. 8 shows that LOI and XARM combinations from intervals 1, 2 and 3 notably group with those of unit 1.

4.5. Geochemistry

Following the previously described selection criteria (paragraph 3.2.6.2), we included elemental count rates of K, Ti, Fe, Rb and Zr in our study to detect changes in lithogenic influx and glacier mass turnover (Bakke et al., 2010; Guyard et al., 2013; Kylander et al., 2011; Vasskog et al., 2012). We used the frequently applied Fe/Ti ratio (Croudace et al., 2006; Cuven et al., 2010; Thomson et al., 2006) to assess the impact of redox diagenesis on the Hajeren record. Fig. 5 demonstrates that Fe/Ti ratios are low and vary little throughout unit 4 and, to a lesser extent, units 1 and 3. Unit 2, on the other hand, displays a notably higher degree of variability while average Fe/Ti ratios are an order of magnitude larger. Fe/Ti mimics LOI throughout units 1, 2 and 3 as attested by a ϱ of 0.81 (n = 533). ARM values also capture Fe/Ti variability, as expected based on the relation between organic content and XARM show in Fig. 8. This correlation is strongest for the 0.5 cm XARM record (ϱ = 0.55, n = 324). As with LOI and ARM, the higher and more variable Fe/Ti ratios of unit 2 also display a similar asymmetrical increase towards maximum values between 50 and 60 cm core depth. This build-up

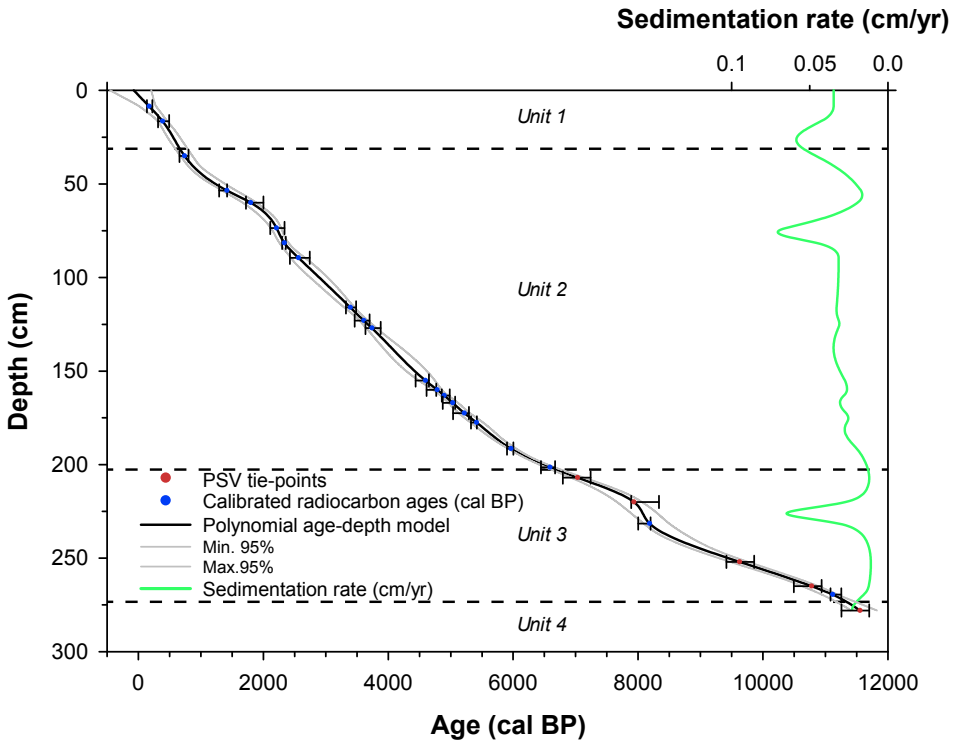

Fig. 6. Age-depth model constructed for core HAP0212, applying polynomial regression on the radiocarbon dates listed in Table 1, indicated by blue dotes. Calibrated age uncertainties are expressed by asymmetrical error bars, while 95% confidence limits are marked by grey lines. Reconstructed sedimentation rates are displayed on the right. (For interpretation of the references to color in this figure legend, the reader is referred to the web version of this article.)

is also interrupted in the Fe/Ti record during intervals 1, 2 and 3 where values are lowest.

We used conservative Titanium (Ti) to detect changes in lithogenic influx and glacier mass turnover following Bakke et al. (2009). Ti elemental count rates were normalized against LOI (paragraph 3.2.6.2) to address the closed-sum effect (Rollison, 1993) and isolate variability not related to changes in sediment organic content. Fig. 4 indicates that down-core Ti/LOI variability bears great resemblance to the previously described DBD record as demonstrated by a Spearman's rho (ϱ) of 0.944 ($n = 616$). Values peak in the course-grained sandy silts of unit 4 and are generally high in the minerogenic silty clays of units 1 and 3. Ti/LOI ratios gradually decrease from the latter unit towards low background values of organic-rich unit 2. As can be seen in Fig. 4, the minerogenic intervals 1, 2 and 3 also show up as marked features in the Ti/LOI record. As with DBD, intervals 2 and 3 are particularly pronounced with values similar to the minerogenic sediments of unit 1. Like DBD, Ti/LOI values are highly variably throughout unit 1. After levelling off after the onset of minerogenic sedimentation, average values decline while displaying a high degree of variability before peaking again around 4 cm depth.

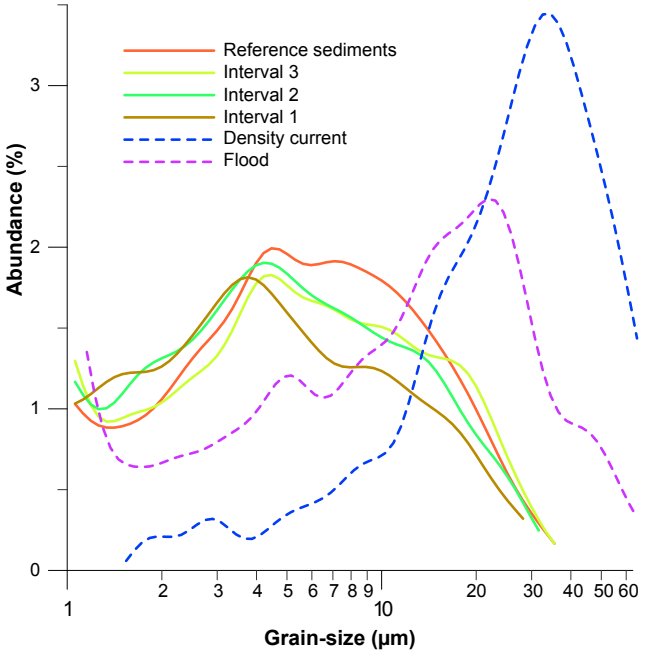

Fig. 7. Grain size distribution data (0–63 µm) plotted on a semi logarithmic scale for minerogenic intervals 1, 2 and 3, compared to LIA sediments (red) as well as common mass-wasting events density currents and floods (dashed) from Vasskog et al. (2011). (For interpretation of the references to color in this figure legend, the reader is referred to the web version of this article.)

4.6. Ordination

To detect common environmental variability in our dataset and help assess whether proxies show a shared response to glacier activity, we carried out PCA following Vasskog et al. (2012) and Bakke et al. (2013). Fig. 9 shows the ensuing ordination diagram with the 9 selected geochemical, physical and magnetic variables. Post-analysis transformation included scaling sample scores using a 0.4 factor, suggested by CANOCO, to further highlight inter-variable correlations. Here, we plotted sample scores along the first two ordination axes (PC1 and PC2) which together capture 84.5% of variation in core HAP0212. PC1 is most significant and explains 70.5% of all variation, signifying strong shared variability between the measured proxies in Hajeren. As demonstrated by

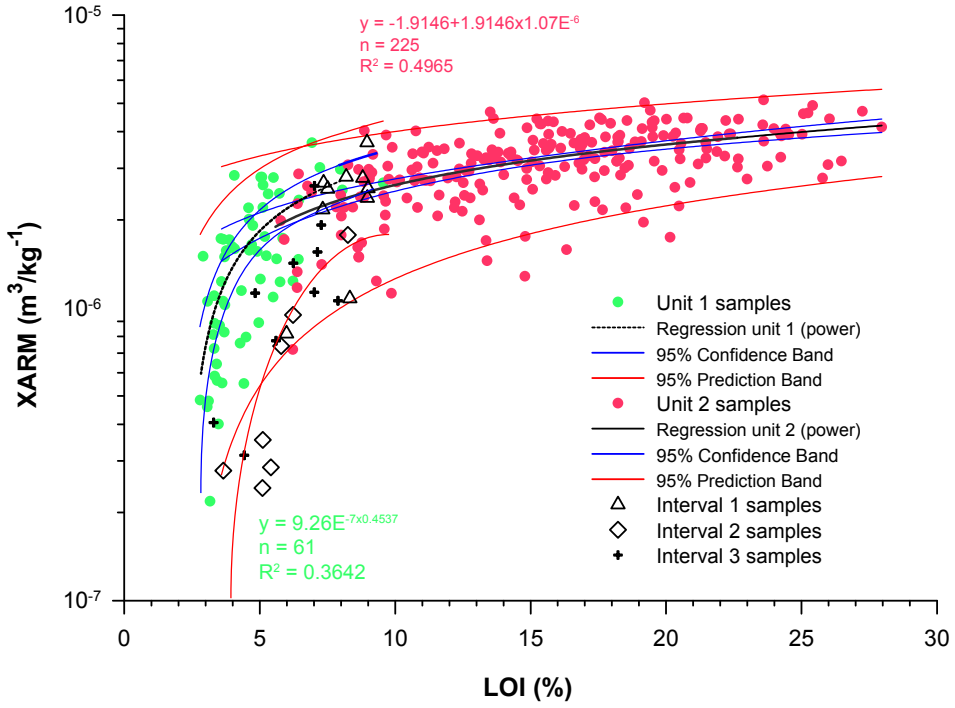

Fig. 8. *X*ARM plotted against LOI on a semi logarithmic scale for samples from units 1 (green), 2 (pink) and minerogenic intervals 1, 2 and 3 (symbols) (n = 327). Regression coefficients emphasize that both groups exhibit different relationship between LOI and *X*ARM. 95% predication and confidence limits are marked by red and blue lines, respectively. (For interpretation of the references to color in this figure legend, the reader is referred to the web version of this article.)

Fig. 9, ordination underlines the robustness of the performed cluster analysis as samples from individual units group together. Samples from the silty clay of units 1 and 3 plot close to PC1 in the lower left quarter of the ordination diagram and are associated with detrital indicators Rb, Zr, Ti and K as well as DBD. Scores for the minerogenic intervals 1, 2 and 3 group near those from units 1 and 3. Samples from the coarse-grained and compacted unit 4 also plot near the DBD vector. Moreover, the distinctness of unit 4 is reflected by the PCA by a relatively strong loading on PC2 and grouping of samples close to the MS vector. Unit 2 samples plot on a gradient along PC1 between the groups of units 1 and 3 towards the correlated variables ARM, LOI and Fe. In general, PC1 covers a gradient of variability between minerogenic indicators (DBD, Rb, Zr, Ti and K) and variables that co-vary with LOI (Fe and ARM).

5. Discussion

5.1. Detection of glacier activity

5.1.1. Sources of error

Understanding catchment processes is imperative for an accurate reconstruction of glacier activity using multi proxy analyses of sediments deposited in distal glacier-fed lakes (Rubensdotter and Rosqvist, 2009; Wittmeier et al., 2015). This is particularly pertinent for processes that may leave a similar physical imprint in lacustrine sediments (Ballantyne, 2002; Leonard, 1997; Rubensdotter and Rosqvist, 2009). Based on the laminated sediments of core HAP0212 and the grain size signature of selected sediments (paragraph 4.3), we suggest that mass wasting events had a limited influence on the Hajeren record. Moreover, a scarcity of mapped fine-grained glacigenic deposits in the catchment indicates that the impact of paraglacial modification is limited (Van der Bilt et al., 2015). This is supported by minimal minerogenic input in unit 2, also suggesting a high sensitivity of the record to the signature of glacial flour.

A site-specific source of error may stem from the presence of two glaciers in the Hajeren catchment (Fig. 1), potentially responding differently to the same climate forcing. However, based on their mapped extent (NPI, 2015), both glaciers show a uniform post-LIA retreat pattern as anticipated based on a corresponding aspect and elevation range. To further assess their individual climate sensitivity, we applied the Hypsometric Index (HI) proposed by Jiskoot et al. (2009) using aerials, a Digital Elevation Model (DEM) and mapped glacier extent (NPI, 2015). Near-identical HI values of 2.13 for the North- and 2.14 for the South Glacier support the notion that both glaciers respond similarly to climate variability.

5.1.2. Multi-proxy approach

Organic content, approximated by LOI, is often used as an inverse indicator of minerogenic sedimentation in glacier-fed lakes to reconstruct glacier activity (Dahl et al., 2003; Karlén, 1976). However, as will be discussed in paragraph 5.2, LOI values in Lake Hajeren do not appear to be governed by minerogenic sedimentation alone, as suggested by a high correlation with redox sensitive Fe/Ti ratios as well as ARM (Fig. 5). Moreover, low (<5%) values during intervals of generally dense minerogenic sedimentation extinguish the amplitude of variation recorded by the LOI record (Bakke et al., 2005; McKay and Kaufman, 2009).

To overcome these limitations, we use DBD to track variations in minerogenic lacustrine input and relate these to past variations in glacier activity. Apart from the influx of minerogenic matter, DBD is affected by variations in grain size. Highest values are found in fine-grained, poorly sorted sediments of low porosity (Menounos, 1997). Glacigenic suspended load is typically dominated by the fine clay and silt fractions (Leemann and Niessen, 1994b). Therefore, lacustrine sediments with a glacial imprint are characterized by a high density as demonstrated by Bakke et al. (2005).

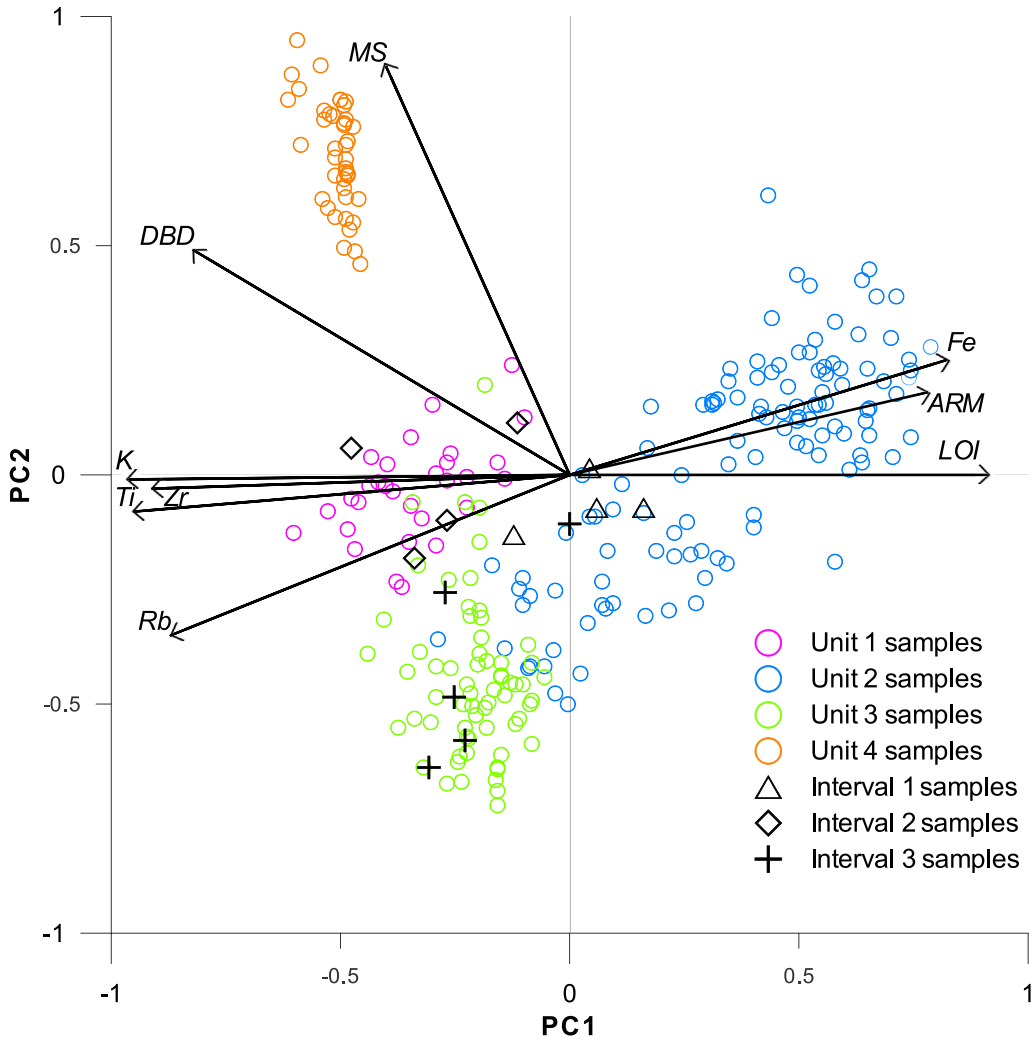

Fig. 9. An ordination diagram, showing the results of PCA on scaled first (PC1) and second (PC2) ordination axes. Open circles represent individual 1 cm resolution down-core samples (n = 250), distinguishing between units using different colors. Samples from minerogenic intervals 1, 2 and 3 are plotted using symbols. Vectors reflect the PCA scores of selected environmental variables.

Following Vasskog et al. (2012) and Wittmeier et al. (2015), we also use PCA to help fingerprint glacigenic sediments. Based on strong loading of DBD and minerogenic indicators Ti, K, Zr and Rb, we argue that PC1 captures the signal of glacier variability in the catchment (Fig. 9). With a loading of −0.945, Ti kcps demonstrate the highest PC1 scores. As such, we validate the physical evidence from DBD variability using concurrent changes in, LOI-normalized (paragraph 3.2.6.2), Ti to detect changes in glacier mass turnover (Bakke et al., 2009) (Fig. 10). Also, samples from unit 1, a period of sustained minerogenic sedimentation and historical glacier activity, group in the same sector of the ordination diagram as DBD and Ti/LOI (Fig. 9).

Finally, the applied multi-proxy toolbox includes grain size analysis on previously described selected minerogenic intervals (Figs. 4 and 7). Quantification of the fine-grained fractions allows additional testing and identification of a glacial signature (Leemann and Niessen, 1994a; Matthews and Karlén, 1992; Peach and Perrie, 1975).

5.2. Non-glacial environmental variability

Minimal minerogenic input is prevalent during the Middle to Late Holocene sediments of unit 2 (Fig. 4). Sediments are mostly organic-rich (Fig. 5) and high LOI correlates strongly with redox-sensitive Fe/Ti ratio (ϱ = 0.68, n = 338), as well as χARM (ϱ = 0.67, n = 256). We argue that, apart from the inferred advances around 4100, 3300 and 1100 cal BP (paragraphs 5.3.3 and 5.3.4) glaciers disappeared from the catchment after ≈ 7.4–6.7 ka cal BP. Instead, it seems plausible that shifting redox conditions in the lake catchment or within the lake itself governed the sedimentation throughout most of unit 2, particularly between ≈4000 and 1400 cal BP. The transition from minerogenic Early Holocene sediments towards core samples that group with LOI and correlated Fe/Ti and ARM values is expressed in the ordination diagram of Fig. 9. Evidently, ARM variability does not co-vary with shifts in minerogenic-derived magnetic grain size in Hajeren as in other glacier-fed lakes (Matthews and Karlén, 1992; Snowball and Sandgren, 1996). Based on the congruous positive relationship seen in Fig. 8, ARM variability in unit 2 appears to be biologically controlled. Though we lack data to detect biogenic magnetite using a Moskowitz diagram (Moskowitz et al., 1993), we tentatively attribute this biological control to Magnetotactic Bacteria (MTB's), following Paasche et al. (2004). These synthesize Magnetite near the Oxic–Anoxic Transition Zone (OATZ) and also occur in adjacent lake Kløsa (Røthe et al., 2015). Coeval high and correlated Fe/Ti ratios, an indicator of redox diagenesis (Croudace et al., 2006;

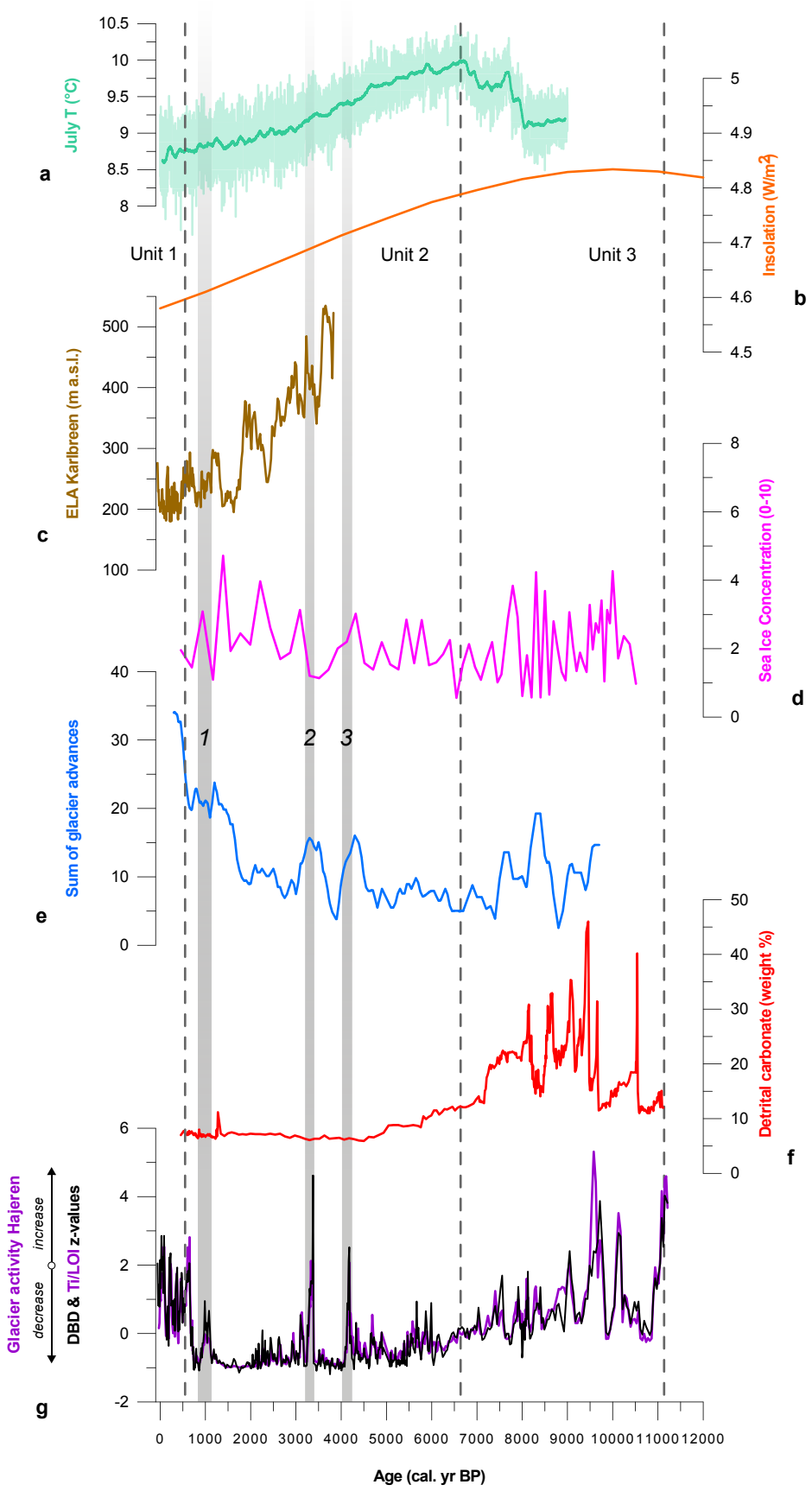

Fig. 10. Comparison between standardized scores of main indicators glacier activity indicators DBD and Ti/LOI from Hajeren (g) and July temperature modelled by Renssen et al. (2009) (a) (opaque line plots raw data, hard line reflects 100 yr running average), summer insolation at 80° North (Huybers, 2006) (b), Equilibrium Altitude Line (ELA)

Cuven et al., 2010), support the prevalence of anoxic conditions.

5.3. Holocene glacier variability

5.3.1. Deglaciation

Distinctly disparate sediment characteristics suggest a different source of the sediments from units 4 and 5 as compared to the rest of the core. This dissimilarity is particularly well expressed by high MS values and captured by the ordination diagram displayed in Fig. 9. In general, high DBD and Ti/LOI values indicate high lithogenic influx in a dynamic setting as demonstrated by the course-grained lithology (Fig. 4). The association of the sandy silts of unit 4 with the underlying diamict and gravel of unit 5 is diagnostic for the transition from ice-contact to distal glacier-fed lake during ice retreat (Ballantyne, 2002). In keeping with this interpretation, we suggest that the diamict of unit 5 is a till, deposited when ice occupied the lake basin. The overlying open-work gravel facies is indicative of sub-aqueous outwash as suggested by Ashley (1995). In summary, following ice retreat, the depositional environment of Hajeren progressively evolved from an ice-contact delta to a more ice-distal setting. The latter gravels progressively fine up into the silty sands of unit 4, suggesting a gradual transition towards a more ice-distal setting (Ballantyne, 2003). The bulk of unit 4 comprises stratified sediments where alternations between silty and sandy beds are recorded by shifts in Ti/LOI (Fig. 4). Such facies are associated with rapid deposition of reworked glacigenic material during deglaciation (Eyles et al., 1990; Müller, 1999). High sedimentation rates are furthermore supported by the presence of dewatering structures. Based on the observed compacted nature of unit 4 deposits, these may also reflect deformation by stranded ice, following Fulton (1965) and Eyles et al. (1991). Overall, we suggest that the sediments of unit 4 and 5 were rapidly deposited during regional deglaciation. Based on the presented age-depth model (Fig. 6), we argue that the Hajeren watershed deglaciated prior to 11,300 cal BP. These findings agree with Landvik et al. (2013), who propose deglaciation of Mitrahalvøya peninsula around 12.2 ka BP.

5.3.2. 11,270–6700 cal BP: Early Holocene glacier activity

All proxy records in Fig. 4 show a steep drop after the transition from unit 4 to 3, indicative of the previously discussed shift in ice proximity and general depositional environment after deglaciation. However, the indicators used to reconstruct glacier activity, DBD and Ti/LOI, show that minerogenic input remains high but variable, with a gradual decrease towards unit 2 (≈6700 cal BP). Moreover, samples from unit 3 have similar ordination scores as those from unit 1 (Fig. 9), deposited during a period of documented glacier activity in the catchment (paragraph 2). Notwithstanding frequent high-amplitude variability, visual inspection of unit 3 reveals a continuous sequence of regularly laminated sediments, suggesting of a low-energy depositional environment.

We therefore argue that glaciers were active in the Hajeren catchment during the Early Holocene. Modification of older glacigenic sediments cannot be excluded (Rubensdotter and Rosqvist, 2009). However, the small catchment size (Fig. 1) (Harbor and Warburton, 1993) and rapid exhaustion of fine-grained deposits (Van der Bilt et al., 2015) argue against prolonged paraglacial activity.

Both indicators of glacier activity as well as sea ice concentration variations in the Fram Strait by de Vernal et al. (2013) indicate a dynamic Early Holocene towards ≈ 9000 cal BP (Fig. 10d and g). This period was characterized by a series of well-expressed high amplitude peaks in glacier activity at 10,130, between 9500 and 9700 and around 9050 cal BP. Timing of these events fall within the uncertainty margin of a ^{10}Be dated moraine at nearby Kongsfjordhallet (Henriksen et al., 2014). Moreover, the most pronounced peak between 9500 and 9700 cal BP coincides with an established Scandinavian glacier advance, known as the Erdalen event (Nesje, 2009). Based on its amplitude and a gradual build-up, we argue this event reflects a Holocene glacier maximum. The mentioned Stage 1 moraines provide geomorphological evidence for a pre-LIA maximum in the Hajeren catchment (Van der Bilt et al., 2015). Strong visual correspondence between the inferred peaks in Early Holocene glacier activity and Labrador shelf Ice Rafted Debris (IRD) spikes (Fig. 10f) (Jennings et al., 2015) hints at forcing by meltwater pulses from the retreating Laurentide Ice Sheet (LIS). This is supported by a maximum cross correlation of 0.42 at a 20 year time lag for the discussed interval. It has been argued that such discharge cooled the North Atlantic by inhibiting meridional overturning circulation (Kaplan and Wolfe, 2006; Thornalley et al., 2009). Fig. 10f illustrates that two of these IRD peaks coincide with the inferred 9500–9700 cal BP glacier maximum in the Hajeren record. Correlation with IRD peaks found at North Atlantic sites more distal to the LIS further underlines the regional climatic significance of this event (Bond et al., 2001).

Following the inferred 9500–9700 cal BP Holocene glacier maximum, the amplitude of inferred events decreased markedly (Fig. 10g). This shift marks the arrival of Atlantic surface waters in the adjacent Kongsfjorden (Rasmussen et al., 2014; Ślubowska-Woldengen et al., 2007), which ameliorated local climate. Subsequent periods of increased glacier activity are less pronounced and minerogenic lacustrine input gradually declines towards unit 2 (Fig. 10g). However, this pattern is notably interrupted by three successive spikes in minerogenic input between ±7900 and 8300 cal BP, simultaneous with an increase in sedimentation rates (Fig. 6). These events fall within the time frame of the well-known 8.2 ka BP event, another climatic perturbation driven by catastrophic meltwater pulses from the melting LIS (Alley and Ágústsdóttir, 2005; Daley et al., 2011; Kleiven et al., 2008). In contrast to other regional records (Wanner et al., 2011), the 8.2 ka BP event does not stand out as a prominent early Holocene climate event in the Hajeren record (Fig. 10g), as previously shown by (Hormes et al., 2009). However, it is argued that the 8.2 ka BP event was characterized by both cold and dry conditions (Rohling and Pälike, 2005; Spurk et al., 2002), and glacier mass balance depends on both temperature and precipitation (Oerlemans, 2005). We argue that arid conditions during the 8.2 ka BP event may have restricted glacier growth in the Hajeren catchment. We theorize that the concurrent reconstructed sea ice maximum (Fig. 10d) may have cut-off marine moisture sources, in keeping with (Müller et al., 2012). Additionally, Greenland ice-core data revealed significant decadal-scale variability during the 8.2 ka BP, with a main event lasting less than 70 years (Thomas et al., 2007), restricting ice accumulation in the Hajeren catchment.

After spiking around 7400 cal BP, minerogenic input steadily decreases towards the transition to unit 2 (Fig. 10g). We therefore argue that glaciers disappeared from the catchment between ≈7400 and 6700 cal BP. This decline is concurrent with a sharp increase in modelled July temperatures towards mid-Holocene peak values (Fig. 10a) by Renssen et al. (2009). This simulation takes the cooling effect of melting LIS remnants into account, which may have helped sustain glacier activity in the Hajeren catchment by delaying and retarding the response to the Holocene summer

reconstruction for adjacent Karlbreen by Røthe et al. (2015) (c), scaled sea-ice concentration from (de Vernal et al., 2013) (d), the sum of reconstructed glacier advances from Wanner et al. (2008) (e) and Labrador shelf Detrital Carbonate Peaks (DCPs) from Jennings et al. (2015) (f). Neoglacial glacier advances 1, 2 and 3 are emphasized using grey bars.

insolation maximum (Fig. 10a and b). Our claim is supported by the onset of undisturbed sedimentation alongside an ice-cored moraine in adjacent Lake Kløsa after 6700 cal BP (Røthe et al., 2015). Moreover, this minimum age estimate of the termination of Early Holocene glacier activity concurs with the transition towards the organic-rich sediments of unit 2 in our record (Fig. 5).

5.3.3. 4250–4050 and 3380–3230 cal BP: Early Neoglacial advances

Mid-Holocene (unit 2) sediments are mostly organic-rich and appear to be governed by non-glacial redox processes (Figs. 5 and 8) (paragraph 5.2). Generally, minerogenic input is minimal as reflected by low DBD and Ti/LOI values (Fig. 4). This pattern is interrupted by the previously discussed minerogenic intervals 3 and 2 (Figs. 4 and 5). Based on multiple lines of proxy evidence, we here argue these represent centennial-scale glacier advances between 4250–4050 and 3380–3230 cal BP, respectively.

During these events, henceforth referred to as advances 3 and 2 (Fig. 10g), the main indicators of glacier activity, Ti/LOI and DBD, peak at values similar to those seen in the Early Holocene (Fig. 10g). This analogy is supported by the grouping of advances 1 and 2 samples with those from units 3 and 1 in the ordination diagram of Fig. 8. Concurrently, declining LOI, (X)ARM and Fe/Ti values (Fig. 5) suggest a waning influence of biological (redox) processes on lake conditions during the discussed intervals (paragraph 5.2). This is also demonstrated by the deviation of LOI/XARM combinations from the inferred biologically driven trend for other Mid-Holocene samples (Fig. 8). Instead, samples from the discussed intervals plot near those from minerogenic unit 1, which comprises sediments from a period of documented historical glacier activity. Though the onset of these advances appears abrupt (Fig. 10g), both lithostratigraphy and radiograph grayscale imagery suggest gradual change, as indicated by the laminated nature of the sediments (Figs. 4 and 5). Also, underrepresentation of coarser fractions suggests these intervals were not deposited by rapid mass-wasting events (Karlén, 1981; Rubensdotter and Rosqvist, 2009) (Fig. 7). Instead, the observed bimodal grain size distribution, with modes in the fine and medium silt fractions, is diagnostic for glacigenic suspended load (Leemann and Niessen, 1994a; Støren et al., 2008; Vasskog et al., 2012).

The proposed centennial-scale cycles of glacier growth and decay are rapid, though not unprecedented. Jóhannesson et al. (1989) infer a response time of decades for small glaciers like those of the Hajeren catchment. Moreover, reconstructed glacier activity at the comparably-sized Kråkenes cirque system shows a similarly fast sequence of formation and disappearance during the Younger Dryas (Bakke et al., 2009; Paasche, 2011). Also, evidence from modelling studies suggests that small and steep glaciers, like those in the Hajeren catchment, generally show a sensitive response to climate shifts (Jiskoot, 2011). Finally, short response time is also supported by photographic evidence of a rapid historical post-LIA retreat of both glaciers in the catchment (NPI, 2015).

Based on marine proxy evidence from the Fram Strait and adjacent Kongsfjorden (Rasmussen et al., 2014; Werner et al., 2013), declining sea-surface temperatures and increased ice-rafting mark the end of the Holocene Hypsithermal on Svalbard after 5000 cal BP. This is corroborated by terrestrial evidence from macrofossil analysis (Birks, 1991), suggesting cooler summers after 4000 cal BP. First evidence of glacier reformation comes from Linnébreen on southwest Spitsbergen, which reformed after 4600 ± 0.2 cal BP (Reusche et al., 2014; Svendsen and Mangerud, 1997). Røthe et al. (2015) suggest that neighboring Karlbreen reformed around 3800 cal BP. As such, the discussed glacier advances in the Hajeren catchment occurred after the onset of Neoglaciation on Svalbard. Moreover, reviews of Holocene glacier variability in the (sub)-Arctic shows that timing of both events is consistent with established advances in Scandinavia (Nesje, 2009), Iceland (Geirsdóttir et al., 2009) as well as Alaska (Barclay et al., 2009) and Canada (Menounos et al., 2009). This is also reflected by a correlation with maxima in reconstructed glacier advances from mostly mid-high latitude sites on the Northern Hemisphere by Wanner et al. (2011), shown in Fig. 10e.

We propose that the interplay between long- and short-term regional forcings created suitable conditions for the discussed centennial-scale glacier advances. The onset of Neoglacial cooling occurred against a background of gradual orbital forced summer cooling as shown in Fig. 10b (Huybers, 2006). Stronger advection of Arctic water, linked to increased sea-ice export through the Fram Strait (Funder et al., 2011; Werner et al., 2013), led to a further deterioration of climate conditions after 5000 cal BP. We argue that this cooling trend progressively lowered the glaciation threshold in the Hajeren catchment, enabling super-imposed shorter-term forcings to create suitable conditions for the discussed advances. Based on their duration and correspondence with regional records of glacier variability (Wanner et al., 2011) (Fig. 10e), we infer a short-term forcing with a North Atlantic signature. This claim is also supported by correlation of the discussed events with peaks in North Atlantic iceberg-derived debris (Bond et al., 1997). Though initially solely attributed to low solar activity (Bond et al., 2001), recent studies highlight the contribution of internal dynamics of the North Atlantic in driving these quasi-cyclic peaks (Debret et al., 2007, 2009; Renssen et al., 2007; Solomina et al., 2015; Wanner et al., 2011).

5.3.4. 3230–700 cal BP: unfavorable conditions for glacier growth

Following the previously discussed short-lived Early Neoglacial glacier advances, minerogenic input drops to a Holocene minimum (Fig. 10g). Based on this evidence, we suggest that glaciers were absent from the catchment between ≈3230 and 1100 cal BP. Though Humlum et al. (2005) also infer ice-free conditions for Longyearbreen glacier before 1100 cal BP, our record differs from other glacier reconstructions from western Svalbard (Reusche et al., 2014; Røthe et al., 2015). These studies propose a glacier maximum around 1700 cal BP. We argue that glacier growth at that time was driven by increased winter precipitation and suppressed in the lower-lying Hajeren catchment cirques by concurrent warm summers.

After 3000 cal BP, marine records from the Fram strait suggest a generally stronger influence of cold Arctic surface waters and increased sea-ice cover (de Vernal et al., 2013; Rasmussen et al., 2014; Werner et al., 2013) (Fig. 10d). Forwick and Vorren (2009) infer shore-fast ice conditions in Isfjorden, South Spitsbergen. Such conditions would have cut off the main moisture source from the maritime glaciers of West Spitsbergen, creating unfavorable conditions for ice growth (Müller et al., 2012). Apart from a short-lived lowering around 2300 cal BP, this is also reflected by a fairly constant reconstructed Equilibrium Line Altitude (ELA) of adjacent Karlbreen (Fig. 10c). However, particularly after 2000 cal BP (Rasmussen et al., 2014), unstable conditions drove episodic, rapid sea-ice fluctuations that increased moisture availability (de Vernal et al., 2013; Liu et al., 2012; Müller et al., 2012) (Fig. 10d). Werner et al. (2013) attribute this shift to episodic strengthening of warmer Atlantic water inflow, ameliorating climate. This is supported by Sarnthein et al. (2003), who infer SST peaks concurrent with the mentioned 2200 cal BP ELA lowering and 1700 cal BP glacier maximum at adjacent Karlbreen. Moreover, D'Andrea et al. (2012) and Kaufman (2009) show relatively high coeval summer air temperatures. Based on the outlined evidence, we concur with Røthe et al. (2015) that increased winter precipitation drove glacier growth at the time. We argue that warm summers offset any gains

in accumulation through increased ablation in the low-lying Hajeren catchment cirques. In short, we suggest that between ≈3230 and 1100 cal BP, conditions in the Hajeren catchment were either too dry or too warm to sustain glacier growth.

Around 1100 cal BP, a sustained peak in Ti/LOI and DBD values during interval 1 marks a shift towards predominantly minerogenic lacustrine sedimentation (Fig. 10g). Though peak values of this interval are subdued compared to the discussed minerogenic intervals, ordination and grain size data suggest a similar signature (Figs. 7 and 9). We therefore argue that interval 1 reflects a period of glacier activity, henceforth referred to as advance 1 (Fig. 10). Timing corresponds to the re-growth of Longyearbreen glacier on southern Svalbard documented by Humlum et al. (2005). Also, Fig. 10c shows a synchronous 100 m lowering of the reconstructed ELA at adjacent Karlbreen. The temperature record of D'Andrea et al. (2012) indicate that the period around 1100 cal BP was characterized by the coolest summers of the past 1800 years. This signals that the discussed advance was temperature-driven as previously suggested by Humlum et al. (2005).

Shortly after 1000 cal BP, minerogenic input drops to background levels (Fig. 10g). This decline coincides with a period marked by high summer temperatures (D'Andrea et al., 2012). We propose that this warming ended the previously discussed advance, represented by interval 1. Subsequently, organic-rich sediments become prevalent (Fig. 5). We argue that this epoch, which lasted until ≈750 cal BP (Fig. 10g), marks the Medieval Climate Anomaly (MCA) (Bradley et al., 2003). These findings agree with Spielhagen et al. (2011) and Grinsted et al. (2006), who reconstruct concurrent summer warming of sub-surface waters and increased ice core melt, respectively.

5.3.5. 700 cal BP-present: Little Ice Age

Unit 1 marks the first prolonged episode of minerogenic sedimentation in Lake Hajeren since ≈7400–6700 cal BP as shown in Figs. 4 and 10g. We propose that the transition into unit 1 marks the onset of the Little Ice Age (LIA) in the Hajeren catchment. Based on sustained high minerogenic input, we argue that glaciers were continuously present after ≈700 cal BP. Coincident minimum ELA's at Karlbreen suggest this time interval was characterized by the most favorable local conditions for glacier growth in at least 3800 years (Fig. 10e and c). Also, Dylmer et al. (2013) demonstrate that this transition is concurrent with a sudden reduction in Atlantic water flow off Svalbard. Timing of LIA glacier growth around 700 cal BP also agrees with the findings of Svendsen and Mangerud (1997) for Linnébreen glacier and Furrer (1991) for Adolfbreen glacier on northwest Spitsbergen. Following with Werner (1993) and Røthe et al. (2015), we observe a two-step LIA in our record with glacier activity peaking around 650 cal BP and again at the close of the 19th century (Fig. 10c and g).

While available records all present evidence for widespread glacier growth on Svalbard during the LIA, its signature remains ambiguous. Müller et al. (2012) infer extensive sea-ice cover for the past 600 years, based on high IP_{25} flux rates. Additionally, Fauria et al. (2010) suggest maximum winter sea-ice extent between the 17th and 19th centuries using ice-core $d^{18}O$ data from Lomonosovfonna. This evidence is supported by low concentrations of marine-derived salt ions from the same site (Grinsted et al., 2006). Furthermore, Spielhagen et al. (2011) reconstructed increasing summer SST's in the Eastern Fram Strait during this period. In line with these findings, D'Andrea et al. (2012) demonstrate a concurrent increase in summer air temperatures. The outlined combination of extensive sea-ice and warm summers would starve glaciers from moisture in winter (Liu et al., 2012; Müller et al., 2012) whilst increasing summer ablation, creating conditions unfavorable for glacier growth (Oerlemans, 2005). Hence, the climatic driver of LIA glacier growth on Svalbard remains elusive and deserves future investigation.

6. Conclusions

This study presents a continuous reconstruction of Holocene glacier variability on Svalbard at centennial timescales, combining physical, geochemical and magnetic proxies with multivariate statistics. Integrating our findings from Lake Hajeren in a regional paleoclimatic context, we observe a three-staged Holocene climate history. Following deglaciation around 11,300 cal BP, glaciers remained present in the catchment throughout the Early Holocene, culminating in a glacier maximum around 9.5 cal BP. During this period, glacier activity appears to be affected by meltwater pulses from the melting LIS (Jennings et al., 2015). Following a late onset of the HTM around 6.7 ka cal BP, in line with modeled cooling effects from the melting LIS (Renssen et al., 2009), glaciers disappear from the catchment. Instead, changing redox conditions driven by stratification of the water column governed lacustrine sedimentation during most of the Middle and Late Holocene. Two advances between 4205–4050 and 3380–3220 cal BP mark the onset of the Neoglacial and coincide with brief episodes of North Atlantic cooling (Bond et al., 2001; Debret et al., 2007; Renssen et al., 2007). A gradual decline in summer insolation progressively lowered the glaciation threshold towards the Late Holocene, resulting in prolonged glacier activity around 700 cal BP. This local onset of the LIA is in line with advances reported at nearby sites (Furrer, 1991; Røthe et al., 2015; Svendsen and Mangerud, 1997; Werner, 1993). The rapid response of the small Hajeren glaciers improves our understanding of climate variability on Svalbard, suggesting that the Holocene was punctuated by major centennial-scale perturbations. As such, this study underlines the value of glacier-fed lake sediments in contextualizing Arctic climate dynamics.

Acknowledgments

This study has received funding from the Norwegian Research Council through the project «Shifting Climate States of the Polar Regions» (210004). This work was also supported by the Norwegian Research Council funded Arctic Field Grant program (Grant, RiS 6663) as well as the Norwegian Research School in Climate Dynamics. We would like to acknowledge Rob D'Anjou, Nicholas Balascio, Marthe Gjerde and Torgeir Røthe for retrieving the studied sediment cores. Finally, we thank our reviewers, Ólafur Ingólfsson and Anne Hormes, for improving this manuscript with their comments.

References

Aagaard-Sørensen, S., Husum, K., Hald, M., Marchitto, T., Godtliebsen, F., 2014. Sub sea surface temperatures in the polar north Atlantic during the Holocene: planktic foraminiferal Mg/Ca temperature reconstructions. Holocene 24, 93–103.

Alley, R.B., Ágústsdóttir, A.M., 2005. The 8k event: cause and consequences of a major Holocene abrupt climate change. Quat. Sci. Rev. 24, 1123–1149.

Ashley, G., 1995. Glaciolacustrine environments. Glacial Environ. 1, 417–444.

Bakke, J., Nesje, A., Dahl, S.O., 2005. Utilizing physical sediment variability in glacier-fed lakes for continuous glacier reconstructions during the Holocene, northern Folgefonna, western Norway. Holocene 15, 161–176.

Bakke, J., Lie, Ø., Heegaard, E., Dokken, T., Haug, G.H., Birks, H.H., Dulski, P., Nilsen, T., 2009. Rapid oceanic and atmospheric changes during the younger Dryas cold period. Nat. Geosci. 2, 202–205.

Bakke, J., Dahl, S.O., Paasche, Ø., Riis Simonsen, J., Kvisvik, B., Bakke, K., Nesje, A., 2010. A complete record of Holocene glacier variability at Austre Okstindbreen, northern Norway: an integrated approach. Quat. Sci. Rev. 29, 1246–1262.

Bakke, J., Trachsel, M., Kvisvik, B.C., Nesje, A., Lysså, A., 2013. Numerical analyses of a multi-proxy data set from a distal glacier-fed lake, Sørsendalsvatn, western Norway. Quat. Sci. Rev. 73, 182–195.

Ballantyne, C.K., 2002. Paraglacial geomorphology. Quat. Sci. Rev. 21, 1935–2017.

Ballantyne, C., 2003. Paraglacial Landsystems. Glacial Landsystems. Arnold, London,

pp. 432–461.
Barclay, D.J., Wiles, G.C., Calkin, P.E., 2009. Holocene glacier fluctuations in Alaska. Quat. Sci. Rev. 28, 2034–2048.
Benestad, R., Hanssen-Bauer, I., Skaugen, T., Førland, E., 2002. Associations between Sea-ice and the Local Climate on Svalbard. Norwegian Meteorological Institute Report, Oslo, pp. 1–7.
Birks, H.H., 1991. Holocene vegetational history and climatic change in west Spitsbergen-plant macrofossils from Skardtjørna, an Arctic lake. Holocene 1, 209–218.
Birks, H., 1998. DG Frey and ES Deevey review 1: numerical tools in palaeolimnology–Progress, potentialities, and problems. J. Paleolimnol. 20, 307–332.
Blaauw, M., 2010. Methods and code for 'classical' age-modelling of radiocarbon sequences. Quat. Geochronol. 5, 512–518.
Blott, S.J., Pye, K., 2001. GRADISTAT: a grain size distribution and statistics package for the analysis of unconsolidated sediments. Earth Surf. Process. Landf. 26, 1237–1248.
Boës, X., Rydberg, J., Martinez-Cortizas, A., Bindler, R., Renberg, I., 2011. Evaluation of conservative lithogenic elements (Ti, Zr, Al, and Rb) to study anthropogenic element enrichments in lake sediments. J. Paleolimnol. 46, 75–87.
Bond, G., Showers, W., Cheseby, M., Lotti, R., Almasi, P., Priore, P., Cullen, H., Hajdas, I., Bonani, G., 1997. A pervasive millennial-scale cycle in North Atlantic Holocene and glacial climates. Science 278, 1257–1266.
Bond, G., Kromer, B., Beer, J., Muscheler, R., Evans, M.N., Showers, W., Hoffmann, S., Lotti-Bond, R., Hajdas, I., Bonani, G., 2001. Persistent solar influence on North Atlantic climate during the Holocene. Science 294, 2130–2136.
Bradley, R.S., Hughes, M.K., Diaz, H.F., 2003. Climate in medieval time. Science 302, 404–405.
Carrivick, J.L., Tweed, F.S., 2013. Proglacial lakes: character, behaviour and geological importance. Quat. Sci. Rev. 78, 34–52.
Croudace, I.W., Rindby, A., Rothwell, R.G., 2006. ITRAX: Description and Evaluation of a New Multi-function X-ray Core Scanner. Spec. Publ.Geol. Soc. Lond. 267, 51.
Cuven, S., Francus, P., Lamoureux, S.F., 2010. Estimation of grain size variability with micro X-ray fluorescence in laminated lacustrine sediments, Cape Bounty, Canadian high Arctic. J. Paleolimnol. 44, 803–817.
Dahl, S.O., Bakke, J., Lie, Ø., Nesje, A., 2003. Reconstruction of former glacier equilibrium-line altitudes based on proglacial sites: an evaluation of approaches and selection of sites. Quat. Sci. Rev. 22, 275–287.
Daley, T.J., Thomas, E.R., Holmes, J.A., Street-Perrott, F.A., Chapman, M.R., Tindall, J.C., Valdes, P.J., Loader, N.J., Marshall, J.D., Wolff, E.W., Hopley, P.J., Atkinson, T., Barber, K.E., Fisher, E.H., Robertson, I., Hughes, P.D.M., Roberts, C.N., 2011. The 8200 yr BP cold event in stable isotope records from the north Atlantic region. Glob. Planet. Change 79, 288–302.
Dallmann, W.K.E., 2015. Geoscience Atlas of Svalbard. Norwegian Polar Institute, Tromsø.
de Vernal, A., Hillaire-Marcel, C., Rochon, A., Frechette, B., Henry, M., Solignac, S., Bonnet, S., 2013. Dinocyst-based reconstructions of sea ice cover concentration during the Holocene in the Arctic Ocean, the northern North Atlantic Ocean and its adjacent seas. Quat. Sci. Rev. 79, 111–121.
Debret, M., Bout-Roumazeilles, V., Grousset, F., Desmet, M., McManus, J.F., Massei, N., Sebag, D., Petit, J.-R., Copard, Y., Trentesaux, A., 2007. The origin of the 1500-year climate cycles in Holocene north-Atlantic records. Clim. Past Discuss. 3, 679–692.
Debret, M., Sebag, D., Crosta, X., Massei, N., Petit, J.-R., Chapron, E., Bout-Roumazeilles, V., 2009. Evidence from wavelet analysis for a mid-Holocene transition in global climate forcing. Quat. Sci. Rev. 28, 2675–2688.
Dylmer, C., Giraudeau, J., Eynaud, F., Husum, K., Vernal, A.D., 2013. Northward advection of Atlantic water in the eastern Nordic seas over the last 3000 yr. Clim. Past 9, 1505–1518.
D'Andrea, W.J., Vaillencourt, D.A., Balascio, N.L., Werner, A., Roof, S.R., Retelle, M., Bradley, R.S., 2012. Mild little Ice age and unprecedented recent warmth in an 1800 year lake sediment record from Svalbard. Geology 40, 1007–1010.
Eyles, N., Mullins, H.T., Hine, A.C., 1990. Thick and fast: sedimentation in a Pleistocene fiord lake of British Columbia, Canada. Geology 18, 1153–1157.
Eyles, N., Mullins, H.T., Hine, A.C., 1991. The seismic stratigraphy of Okanagan Lake, British Columbia; a record of rapid deglaciation in a deep 'fiord-lake' basin. Sediment. Geol. 73, 13–41.
Fauria, M.M., Grinsted, A., Helama, S., Moore, J., Timonen, M., Martma, T., Isaksson, E., Eronen, M., 2010. Unprecedented low twentieth century winter sea ice extent in the western Nordic seas since AD 1200. Clim. Dyn. 34, 781–795.
Folk, R.L., Ward, W.C., 1957. Brazos river bar: a study in the significance of grain size parameters. J. Sediment. Res. 27.
Førland, E.J., Benestad, R., Hanssen-Bauer, I., Haugen, J.E., Skaugen, T.E., 2012. Temperature and precipitation development at Svalbard 1900–2100. Adv. Meteorol. 2011.
Forwick, M., Vorren, T.O., 2009. Late Weichselian and Holocene sedimentary environments and ice rafting in Isfjorden, Spitsbergen. Palaeogeogr. Palaeoclimatol. Palaeoecol. 280, 258–274.
Fulton, R.J., 1965. Silt deposition in late-glacial lakes of southern British Columbia. Am. J. Sci. 263, 553–570.
Funder, S., Goosse, H., Jepsen, H., Kaas, E., Kjær, K.H., Korsgaard, N.J., Larsen, N.K., Linderson, H., Lysså, A., Möller, P., 2011. A 10,000-year record of Arctic Ocean sea-ice variability—view from the beach. Science 333, 747–750.
Furrer, G., 1991. Zum Alter Waamoränen um das Vorfeld des Erikbreen und auf der westlichsten Lernerinsel - ein Beitrag zur Gletchergeschichte des Liefdesfjords. In: Sonderveröffentlichungen, 21. Geologisches Institut der Universität zu Köln.
Geirsdóttir, Á., Miller, G.H., Axford, Y., Sædís, Ó., 2009. Holocene and latest Pleistocene climate and glacier fluctuations in Iceland. Quat. Sci. Rev. 28, 2107–2118.
Grimm, E.C., 1987. CONISS: a FORTRAN 77 program for stratigraphically constrained cluster analysis by the method of incremental sum of squares. Comput. Geosci. 13, 13–35.
Grimm, E., 2011. Tilia Software V. 1.7. 16. Illinois State Museum, Springfield.
Grinsted, A., Moore, J.C., Pohjola, V., Martma, T., Isaksson, E., 2006. Svalbard summer melting, continentality, and sea ice extent from the Lomonosovfonna ice core. J. Geophys. Res. Atmos. (1984–2012) 111.
Guyard, H., Chapron, E., St-Onge, G., Labrie, J., 2013. Late-Holocene NAO and ocean forcing on high-altitude proglacial sedimentation (Lake Bramant, western French Alps). Holocene 23 (8), 1163–1172.
Harbor, J., Warburton, J., 1993. Relative rates of glacial and nonglacial erosion in alpine environments. Arct. Alp. Res. 1–7.
Heiri, O., Lotter, A.F., Lemcke, G., 2001. Loss on ignition as a method for estimating organic and carbonate content in sediments: reproducibility and comparability of results. J. Paleolimnol. 25, 101–110.
Henriksen, M., Alexanderson, H., Landvik, J.Y., Linge, H., Peterson, G., 2014. Dynamics and retreat of the late Weichselian Kongsfjorden ice stream, NW Svalbard. Quat. Sci. Rev. 92, 235–245.
Hormes, A., Blaauw, M., Dahl, S.O., Nesje, A., Possnert, G., 2009. Radiocarbon wiggle-match dating of proglacial lake sediments–Implications for the 8.2 ka event. Quat. Geochronol. 4, 267–277.
Hotelling, H., 1933. Analysis of a complex of statistical variables into principal components. J. Educ. Psychol. 24, 417.
Humlum, O., Elberling, B., Hormes, A., Fjordheim, K., Hansen, O.H., Heinemeier, J., 2005. Late-Holocene glacier growth in Svalbard, documented by subglacial relict vegetation and living soil microbes. Holocene 15, 396–407.
Huybers, P., 2006. Early Pleistocene glacial cycles and the integrated summer insolation forcing. Science 313, 508–511.
Jennings, A., Andrews, J., Pearce, C., Wilson, L., Ólafsdóttir, S., 2015. Detrital carbonate peaks on the Labrador shelf, a 13–7 ka template for freshwater forcing from the Hudson Strait outlet of the Laurentide Ice sheet into the subpolar gyre. Quat. Sci. Rev. 107, 62–80.
Jiskoot, H., 2011. Dynamics of Glaciers, Encyclopedia of Snow, Ice and Glaciers. Springer, pp. 245–256.
Jiskoot, H., Curran, C.J., Tessler, D.L., Shenton, L.R., 2009. Changes in Clemenceau Icefield and Chaba group glaciers, Canada, related to hypsometry, tributary detachment, length–slope and area–aspect relations. Ann. Glaciol. 50, 133–143.
Jóhannesson, T., Raymond, C.F., Waddington, E.D., 1989. A simple method for determining the response time of glaciers. In: Oerlemans, J. (Ed.), Glacier Fluctuations and Climatic Change. Springer, Netherlands, pp. 343–352.
Jones, K.P.N., McCave, I.N., Patel, D., 1988. A computer-interfaced sedigraph for modal size analysis of fine-grained sediment. Sedimentology 35, 163–172.
Kaplan, M.R., Wolfe, A.P., 2006. Spatial and temporal variability of Holocene temperature in the North Atlantic region. Quat. Res. 65, 223–231.
Karlén, W., 1976. Lacustrine sediments and tree-limit variations as indicators of Holocene climatic fluctuations in Lappland, northern Sweden. Geogr. Ann. Ser. A. Phys. Geogr. 1–34.
Karlén, W., 1981. Lacustrine sediment studies. A technique to obtain a continous record of holocene glacier variations. Geogr. Ann. Ser. A. Phys. Geogr. 273–281.
Kaufman, D.S., 2009. An overview of late Holocene climate and environmental change inferred from Arctic lake sediment. J. Paleolimnol. 41, 1–6.
Kleiven, H.K.F., Kissel, C., Laj, C., Ninnemann, U.S., Richter, T.O., Cortijo, E., 2008. Reduced North Atlantic deep water coeval with the glacial Lake Agassiz freshwater outburst. Science 319, 60–64.
Koinig, K.A., Shotyk, W., Lotter, A.F., Ohlendorf, C., Sturm, M., 2003. 9000 years of geochemical evolution of lithogenic major and trace elements in the sediment of an alpine lake–the role of climate, vegetation, and land-use history. J. Paleolimnol. 30, 307–320.
Krasilščikov, A., 1975. Stratigraphy and tectonics of the Precambrian of Svalbard, the geological development of Svalbard during the Precambrian, lower Palaeozoic, and Devonian. In: Symposium on Svalbard's Geology. Oslo, pp. 2–5.
Kylander, M.E., Ampel, L., Wohlfarth, B., Veres, D., 2011. High-resolution X-ray fluorescence core scanning analysis of Les Echets (France) sedimentary sequence: new insights from chemical proxies. J. Quat. Sci. 26, 109–117.
Lamoureux, S., Gilbert, R., 2004. Physical and chemical properties and proxies of high latitude lake sediments. In: Smol, J., Pienitz, R., Douglas, M.V. (Eds.), Long-term Environmental Change in Arctic and Antarctic Lakes. Springer, Netherlands, pp. 53–87.
Landvik, J.Y., Brook, E.J., Gualtieri, L., Linge, H., Raisbeck, G., Salvigsen, O., Yiou, F., 2013. 10Be exposure age constraints on the late Weichselian ice-sheet geometry and dynamics in inter-ice-stream areas, western Svalbard. Boreas 42, 43–56.
Larsen, D.J., Miller, G.H., Geirsdóttir, Á., Ólafsdóttir, S., 2012. Non-linear Holocene climate evolution in the North Atlantic: a high-resolution, multi-proxy record of glacier activity and environmental change from Hvítárvatn, central Iceland. Quat. Sci. Rev. 39, 14–25.
Leemann, A., Niessen, F., 1994a. Holocene glacial activity and climatic variations in the Swiss Alps: reconstructing a continuous record from proglacial lake sediments. Holocene 4, 259–268.
Leemann, A., Niessen, F., 1994b. Varve formation and the climatic record in an Alpine proglacial lake: calibrating annually-laminated sediments against hydrological and meteorological data. Holocene 4, 1–8.
Legendre, P., Birks, H.J.B., 2012. From Classical to Canonical Ordination, Tracking

Environmental Change Using Lake Sediments. Springer, pp. 201–248.
Leonard, E.M., 1985. Glaciological and climatic controls on lake sedimentation, Canadian Rocky Mountains. Z. Gletscherkd. Glazialgeol. 21, 35–42.
Leonard, E.M., 1997. The relationship between glacial activity and sediment production: evidence from a 4450-year varve record of neoglacial sedimentation in Hector Lake, Alberta, Canada. J. Paleolimnol. 17, 319–330.
Liermann, S., Beylich, A.A., van Welden, A., 2012. Contemporary suspended sediment transfer and accumulation processes in the small proglacial Sætrevatnet sub-catchment, Bødalen, western Norway. Geomorphology 167–168, 91–101.
Liu, J., Curry, J.A., Wang, H., Song, M., Horton, R.M., 2012. Impact of declining Arctic sea ice on winter snowfall. Proc. Natl. Acad. Sci. 109, 4074–4079.
Loeng, H., 1991. Features of the physical oceanographic conditions of the Barents Sea. Polar Res. 10, 5–18.
Löwemark, L., Chen, H.-F., Yang, T.-N., Kylander, M., Yu, E.-F., Hsu, Y.-W., Lee, T.-Q., Song, S.-R., Jarvis, S., 2011. Normalizing XRF-scanner data: a cautionary note on the interpretation of high-resolution records from organic-rich lakes. J. Asian Earth Sci. 40, 1250–1256.
Matthews, J.A., Karlén, W., 1992. Asynchronous neoglaciation and Holocene climatic change reconstructed from Norwegian glaciolacustrine sedimentary sequences. Geology 20, 991–994.
McGuire, A.D., Chapin, F.S., Walsh, J.E., Wirth, C., 2006. Integrated regional changes in arctic climate Feedbacks: implications for the global climate system. Annu. Rev. Environ. Resour. 31, 61–91.
McKay, N.P., Kaufman, D.S., 2009. Holocene climate and glacier variability at Hallet and Greyling Lakes, Chugach Mountains, south-central Alaska. J. Paleolimnol. 41, 143–159.
McKay, N.P., Kaufman, D.S., 2014. An extended Arctic proxy temperature database for the past 2,000 years. Sci. Data 1.
Menounos, B., 1997. The water content of lake sediments and its relationship to other physical parameters: an alpine case study. Holocene 7, 207–212.
Menounos, B., Osborn, G., Clague, J.J., Luckman, B.H., 2009. Latest Pleistocene and Holocene glacier fluctuations in western Canada. Quat. Sci. Rev. 28, 2049–2074.
Miller, G.H., Alley, R.B., Brigham-Grette, J., Fitzpatrick, J.J., Polyak, L., Serreze, M.C., White, J.W.C., 2010. Arctic amplification: can the past constrain the future? Quat. Sci. Rev. 29, 1779–1790.
Montgomery, D.C., 2008. Design and Analysis of Experiments. John Wiley & Sons.
Moskowitz, B.M., Frankel, R.B., Bazylinski, D.A., 1993. Rock magnetic criteria for the detection of biogenic magnetite. Earth Planet. Sci. Lett. 120, 283–300.
Müller, B.U., 1999. Paraglacial sedimentation and denudation processes in an Alpine valley of Switzerland. An approach to the quantification of sediment budgets. Geodin. Acta 12, 291–301.
Müller, J., Werner, K., Stein, R., Fahl, K., Moros, M., Jansen, E., 2012. Holocene cooling culminates in sea ice oscillations in Fram Strait. Quat. Sci. Rev. 47, 1–14.
Munsell, A.H., Color, M., 2000. Munsell Soil Color Charts. Munsell Color.
Nesje, A., 1992. A piston corer for lacustrine and marine sediments. Arct. Alp. Res. 257–259.
Nesje, A., 2009. Latest Pleistocene and Holocene alpine glacier fluctuations in Scandinavia. Quat. Sci. Rev. 28, 2119–2136.
Nordli, Ø., 2010. The Svalbard airport temperature series. Bulletin of Geography. Phys. Geogr. Ser. 5–25.
Nordli, Ø., Przybylak, R., Ogilvie, A.E., Isaksen, K., 2014. Long-term temperature trends and variability on Spitsbergen: the extended Svalbard airport temperature series, 1898–2012. Polar Res. 33.
NPI, 1936. s36_2066, in: s. dpi. (Ed.). NPI, Svalbard.
NPI, 2009. 2009, in: 13822 (Ed.). Norwegian Polar Institute.
NPI, 2015. Svalbardkartet.
Oerlemans, J., 2005. Extracting a climate signal from 169 glacier records. Science 308, 675–677.
Ohta, Y., Larionov, A.N., Tebenkov, A.M., Lepvrier, C., Maluski, H., Lange, M., Hellebrandt, B., 2002. Single-zircon Pb-evaporation and 40Ar/39Ar dating of the metamorphic and granitic rocks in north-west Spitsbergen. Polar Res. 21, 73–89.
Ólafsdóttir, S., Geirsdóttir, Á., Miller, G.H., Stoner, J.S., Channell, J.E., 2013. Synchronizing Holocene lacustrine and marine sediment records using paleomagnetic secular variation. Geology 41, 535–538.
Østrem, G., Liestøl, O., 1964. Glaciological investigations in Norway 1963. Nor. Geogr. Tidsskr. 18, 281–340.
Overpeck, J., Hughen, K., Hardy, D., Bradley, R., Case, R., Douglas, M., Finney, B., Gajewski, K., Jacoby, G., Jennings, A., 1997. Arctic environmental change of the last four centuries. Science 278, 1251–1256.
Paasche, Ø., 2011. Cirque glaciers. In: Singh, V.P., Singh, P., Haritashya, U.K. (Eds.), Encyclopedia of Snow, Ice and Glaciers. Springer, pp. 141–144.
Paasche, Ø., Løvlie, R., Dahl, S.O., Bakke, J., Nesje, A., 2004. Bacterial magnetite in lake sediments: late glacial to Holocene climate and sedimentary changes in northern Norway. Earth Planet. Sci. Lett. 223, 319–333.
Paasche, Ø., Olaf Dahl, S., Bakke, J., Løvlie, R., Nesje, A., 2007. Cirque glacier activity in arctic Norway during the last deglaciation. Quat. Res. 68, 387–399.
Peach, P.A., Perrie, L.A., 1975. Grain-size distribution within glacial varves. Geology 3, 43–46.
Pithan, F., Mauritsen, T., 2014. Arctic amplification dominated by temperature feedbacks in contemporary climate models. Nat. Geosci. 7, 181–184.
Rasmussen, T.L., Thomsen, E., Skirbekk, K., Ślubowska-Woldengen, M., Klitgaard Kristensen, D., Koç, N., 2014. Spatial and temporal distribution of Holocene temperature maxima in the northern Nordic seas: interplay of Atlantic-, Arctic- and polar water masses. Quat. Sci. Rev. 92, 280–291.
RCoreTeam, 2014. R: a Language and Environment for Statistical Computing. R Foundation for Statistical Computing, Vienna, Austria, 2012. Open access available at: http://cran.r-project.org.
Reimer, P.J., Bard, E., Bayliss, A., Beck, J.W., Blackwell, P.G., Ramsey, C.B., Buck, C.E., Cheng, H., Edwards, R.L., Friedrich, M., 2013. IntCal13 and Marine13 radiocarbon age calibration curves 0–50,000 years cal BP. Radiocarbon 55, 1869–1887.
Renssen, H., Goosse, H., Fichefet, T., 2007. Simulation of Holocene cooling events in a coupled climate model. Quat. Sci. Rev. 26, 2019–2029.
Renssen, H., Seppä, H., Heiri, O., Roche, D., Goosse, H., Fichefet, T., 2009. The spatial and temporal complexity of the Holocene thermal maximum. Nat. Geosci. 2, 411–414.
Reusche, M., Winsor, K., Carlson, A.E., Marcott, S.A., Rood, D.H., Novak, A., Roof, S., Retelle, M., Werner, A., Caffee, M., 2014. ^{10}Be surface exposure ages on the late-Pleistocene and Holocene history of Linnébreen on Svalbard. Quat. Sci. Rev. 89, 5–12.
Richards, J., Moore, R.D., Forrest, A.L., 2012. Late-summer thermal regime of a small proglacial lake. Hydrol. Process. 26, 2687–2695.
Rohling, E.J., Pälike, H., 2005. Centennial-scale climate cooling with a sudden cold event around 8,200 years ago. Nature 434, 975–979.
Roland, E., Haakensen, N., 1985. Glasiologiske Undersøkelser I Norge 1982 (Rapport-Norges Vassdrags-og Elektrisitetsvesen, Hydrologisk Avdeling).
Rollison, H.R., 1993. Using Geochemical Data: Evaluation, Presentation. Interpretation. Longan Scientific and Technical Press, New York.
Rosqvist, G.C., Schuber, P., 2003. Millennial-scale climate changes on south Georgia, southern ocean. Quat. Res. 59, 470–475.
Røthe, T.O., Bakke, J., Vasskog, K., Gjerde, M., D'Andrea, W.J., Bradley, R.S., 2015. Arctic Holocene glacier fluctuations reconstructed from lake sediments at Mitrahalvøya, Spitsbergen. Quat. Sci. Rev. 109, 111–125.
Rubensdotter, L., Rosqvist, G., 2009. Influence of geomorphological setting, fluvial-, glaciofluvial-and mass-movement processes on sedimentation in alpine lakes. Holocene 19, 665–678.
Salvigsen, O., Høgvard, K., 2006. Glacial history, Holocene shoreline displacement and palaeoclimate based on radiocarbon ages in the area of Bockfjorden, northwestern Spitsbergen, Svalbard. Polar Res. 25, 15–24.
Sarnthein, M., Kreveld, S., Erlenkeuser, H., Grootes, P., Kucera, M., Pflaumann, U., Schulz, M., 2003. Centennial-to-millennial-scale periodicities of Holocene climate and sediment injections off the western Barents shelf, 75 N. Boreas 32, 447–461.
Screen, J.A., Simmonds, I., 2010. The central role of diminishing sea ice in recent Arctic temperature amplification. Nature 464, 1334–1337.
Sergeeva, L., 1983. Trace element associations as indicators of sediment accumulation in lakes. In: Meriläinen, J., Huttunen, P., Battarbee, R.W. (Eds.), Paleolimnology. Springer, Netherlands, pp. 81–84.
Serreze, M.C., Barry, R.G., 2011. Processes and impacts of Arctic amplification: a research synthesis. Glob. Planet. Change 77, 85–96.
Simonneau, A., Chapron, E., Garçon, M., Winiarski, T., Graz, Y., Chauvel, C., Debret, M., Motelica-Heino, M., Desmet, M., Di Giovanni, C., 2014. Tracking Holocene glacial and high-altitude alpine environments fluctuations from minerogenic and organic markers in proglacial lake sediments (Lake Blanc Huez, Western French Alps). Quat. Sci. Rev. 89, 27–43.
Ślubowska-Woldengen, M., Rasmussen, T.L., Koç, N., Klitgaard-Kristensen, D., Nilsen, F., Solheim, A., 2007. Advection of Atlantic water to the western and northern Svalbard shelf since 17,500 calyr BP. Quat. Sci. Rev. 26, 463–478.
Šmilauer, P., Lepš, J., 2014. Multivariate Analysis of Ecological Data Using CANOCO 5. Cambridge University Press.
Snowball, I., Sandgren, P., 1996. Lake sediment studies of Holocene glacial activity in the Kårsa valley, northern Sweden: contrasts in interpretation. Holocene 6, 367–372.
Solomina, O.N., Bradley, R.S., Hodgson, D.A., Ivy-Ochs, S., Jomelli, V., Mackintosh, A.N., Nesje, A., Owen, L.A., Wanner, H., Wiles, G.C., 2015. Holocene glacier fluctuations. Quat. Sci. Rev. 111, 9–34.
Solomon, S., 2007. Climate Change 2007-the Physical Science Basis: Working Group I Contribution to the Fourth Assessment Report of the IPCC. Cambridge University Press.
Spielhagen, R.F., Werner, K., Sørensen, S.A., Zamelczyk, K., Kandiano, E., Budeus, G., Husum, K., Marchitto, T.M., Hald, M., 2011. Enhanced modern heat transfer to the Arctic by warm Atlantic water. Science 331, 450–453.
Spurk, M., Leuschner, H.H., Baillie, M.G.L., Briffa, K.R., Friedrich, M., 2002. Depositional frequency of German subfossil oaks: climatically and non-climatically induced fluctuations in the Holocene. Holocene 12, 707–715.
Stoner, J.S., Jennings, A., Kristjánsdóttir, G.B., Dunhill, G., Andrews, J.T., Hardardóttir, J., 2007. A paleomagnetic approach toward refining Holocene radiocarbon-based chronologies: paleoceanographic records from the north Iceland (MD99-2269) and east Greenland (MD99-2322) margins. Paleoceanography 22, PA1209.
Støren, E.N., Dahl, S.O., Lie, Ø., 2008. Separation of late-Holocene episodic paraglacial events and glacier fluctuations in eastern Jotunheimen, central southern Norway. Holocene 18, 1179–1191.
Striberger, J., Björk, S., Ingólfsson, Ó., Kjær, K.H., Snowball, I., Uvo, C.B., 2011. Climate variability and glacial processes in eastern Iceland during the past 700 years based on varved lake sediments. Boreas 40, 28–45.
Sundqvist, H., Kaufman, D., McKay, N., Balascio, N., Briner, J., Cwynar, L., Sejrup, H., Seppä, H., Subetto, D., Andrews, J., 2014. Arctic Holocene proxy climate database–new approaches to assessing geochronological accuracy and encoding climate variables. Clim. Past Discuss. 10, 1–63.

Svendsen, J.I., Mangerud, J., 1997. Holocene glacial and climatic variations on Spitsbergen, Svalbard. Holocene 7, 45–57.
Tanaka, H., Hirabayashi, H., Matsuoka, T., Kaneko, H., 2012. Use of fall cone test as measurement of shear strength for soft clay materials. Soils Found. 52, 590–599.
Ter Braak, C., 1988. CANOCO-a FORTRAN Programme for Canonical Community Ordination by [partial][detrended][canonical] Correspondence Analysis, Principal Components Analysis and Redundancy Analysis (Version 2.1). Agricultural Mathematics Group.
Thomas, E.R., Wolff, E.W., Mulvaney, R., Steffensen, J.P., Johnsen, S.J., Arrowsmith, C., White, J.W., Vaughn, B., Popp, T., 2007. The 8.2 ka event from Greenland ice cores. Quat. Sci. Rev. 26, 70–81.
Thompson, R., Turner, G., 1979. British geomagnetic master curve 10,000-0 yr BP for dating European sediments. Geophys. Res. Lett. 6, 249–252.
Thomson, J., Croudace, I.W., Rothwell, R.G., 2006. A Geochemical Application of the ITRAX Scanner to a Sediment Core Containing Eastern Mediterranean Sapropel Units. Geol. Soc. Lond. Spec. Publ. 267, 65–77.
Thornalley, D.J.R., Elderfield, H., McCave, I.N., 2009. Holocene oscillations in temperature and salinity of the surface subpolar North Atlantic. Nature 457, 711–714.
Tjallingii, R., Röhl, U., Kölling, M., Bickert, T., 2007. Influence of the water content on X-ray fluorescence core-scanning measurements in soft marine sediments. Geochem. Geophys. Geosyst. 8.
Van der Bilt, W.G., Bakke, J., Balascio, N.L., 2015. Mapping Sediment-landform Assemblages to Constrain the Impact of Paraglacial Modification on Sedimentation in a Glacier-fed Lake on Northwest Spitsbergen. J. Maps. ISSN: 1744-5647 (under review).
Vasskog, K., Nesje, A., Støren, E.N., Waldmann, N., Chapron, E., Ariztegui, D., 2011. A Holocene record of snow-avalanche and flood activity reconstructed from a lacustrine sedimentary sequence in Oldevatnet, western Norway. Holocene 21 (4), 597–614, 0959683610391316.
Vasskog, K., Paasche, Ø., Nesje, A., Boyle, J.F., Birks, H.J.B., 2012. A new approach for reconstructing glacier variability based on lake sediments recording input from more than one glacier. Quat. Res. 77, 192–204.
Wanner, H., Beer, J., Bütikofer, J., Crowley, T.J., Cubasch, U., Flückiger, J., Goosse, H., Grosjean, M., Joos, F., Kaplan, J.O., 2008. Mid-to late Holocene climate change: an overview. Quat. Sci. Rev. 27, 1791–1828.
Wanner, H., Solomina, O., Grosjean, M., Ritz, S.P., Jetel, M., 2011. Structure and origin of Holocene cold events. Quat. Sci. Rev. 30, 3109–3123.
Werner, A., 1993. Holocene moraine chronology, Spitsbergen, Svalbard: lichenometric evidence for multiple Neoglacial advances in the Arctic. Holocene 3, 128–137.
Werner, K., Spielhagen, R.F., Bauch, D., Hass, H.C., Kandiano, E., 2013. Atlantic water advection versus sea-ice advances in the eastern Fram Strait during the last 9 ka: multiproxy evidence for a two-phase Holocene. Paleoceanography 28, 283–295.
Wittmeier, H.E., Bakke, J., Vasskog, K., Trachsel, M., 2015. Reconstructing Holocene glacier activity at Langfjordjøkelen, Arctic Norway, using multi-proxy fingerprinting of distal glacier-fed lake sediments. Quat. Sci. Rev. 114, 78–99.